2 The Role of Nanoparticle Suspensions in Thermo/Fluid and Biomedical Applications

Khalil M. Khanafer and Kambiz Vafai

CONTENTS

2.1 INTRODUCTION

Recent advances in nanomaterials and nanotechnology have led to the development of new class of heat-transfer fluids containing nanometer-sized particles called nanoparticles typically made of carbon nanotubes, metals, or oxides. Nanofluids are engineered by suspending nanoparticles with average sizes below 100 nm in

a base fluid such as water, ethylene glycol, and oil [1]. Compared with the base fluid, nanofluids have distinctive properties that make them attractive in many applications such as pharmaceutical processes, transportation industry, thermal management of electronics, fuel cells, boiler flue gas temperature reduction, heat exchangers, etc. [2]. Extensive research studies on heat-transfer enhancement using nanofluids were conducted both experimentally and theoretically in the literature [1–15]. Conflicting results on the heat transfer enhancement using nanofluids in forced and natural convection are reported in the literature. Pak and Cho [16] illustrated that the Nusselt number for Al_2O_3–water and TiO_2–water nanofluids increased with increasing Reynolds number and volume fraction of nanoparticles. Nevertheless, the convective heat-transfer coefficient for nanofluids at a volume fraction of 3% was found to be 12% smaller than that of the base fluid when assuming a constant average velocity [16]. Yang et al. [17] studied experimentally the convective heat-transfer coefficients of graphite–water nanofluids under laminar flow in a horizontal tube heat exchanger. Their experimental heat-transfer coefficients showed that the nanoparticles increased the heat-transfer coefficient of the fluid system in laminar flow, but the increase was much less than that predicted by the existing correlation based on static thermal conductivity measurements. However, many other researchers have reported forced convective heat-transfer enhancement using nanofluids [18–22].

Not many studies are found in the literature on the application of nanofluids in natural convective heat transfer. Khanafer et al. [6] analyzed numerically natural convection heat transfer of nanofluids in an enclosure under various physical parameters. Their results showed that the average Nusselt number increases with an increase in the nanoparticles volume fraction for different Grashof numbers. Kim et al. [23] introduced a factor to explain the effect of nanoparticle addition on the convective instability and heat-transfer characteristics of a base fluid. The new factor included the effect of the ratio of the thermal conductivity of nanoparticles to that of the base fluid, the shape factor of the nanoparticles, the volume fraction of nanoparticles, and the heat capacity ratio. Their results indicate that the heat-transfer coefficient in the presence of nanofluids increases with an increase in the volume fraction of nanoparticles. Ghasemi and Aminossadati [24] numerically studied natural convection heat transfer in an inclined enclosure filled with a CuO–water nanofluid for various pertinent parameters such as Rayleigh number, inclination angle, and solid volume fraction. Their results indicated that the addition of nanoparticles improves heat-transfer performance. In addition, they showed that there is an optimum solid volume fraction that maximizes heat-transfer rate. Natural convective heat-transfer enhancement using nanofluids was also demonstrated experimentally by Nnanna et al. [25] and Nnanna and Routhu [26].

Conversely, Putra et al. [13] illustrated experimentally that the presence of nanoparticles (Al_2O_3 and CuO) in water-based nanofluids inside a horizontal cylinder decreased natural convective heat-transfer coefficient with an increase in the volume fraction of nanoparticles, particle density as well as the aspect ratio of the cylinder. Ding et al. [27] have also reported experimentally that the natural

convective heat-transfer coefficient decreases systematically with an increase in nanoparticle concentration, and the deterioration was partially related to the higher viscosity of nanofluids. Chang et al. [28] considered natural convection experiments with Al_2O_3 micro-particle (approximately 250 nm) aqueous suspensions in thin enclosures. Their results illustrated that nanoparticles have insignificant effect on the Nusselt number values for a vertical enclosure. Nevertheless, for horizontal enclosure, there was a decrease in Nusselt number compared with pure water at lower Rayleigh numbers and higher particle concentrations. The researchers attributed this anomalous behavior to sedimentation.

Presently, there are no robust theoretical models to determine the anomalous thermal conductivity enhancement of nanofluids. Many researchers have attributed the thermal conductivity enhancement of nanofluids to thermal conductivities of fluid and nanoparticles, shape and surface area of nanoparticles, volume fraction, and temperature [29]. Keblinski et al. [29] and Eastman et al. [30] proposed four main mechanisms for thermal conductivity enhancement of nanofluids. These consist of Brownian motion of nanoparticles, molecular-level layering of the liquid at the liquid/particle interface, heat transport within the nanoparticles, and the effects of nanoparticle clustering. On the basis of molecular dynamics simulations and the simple kinetic theory, Evans et al. [31] demonstrated that the hydrodynamics effects associated with Brownian motion have a small effect on the thermal conductivity of the nanofluid. Conflicting results were reported in the literature associated with the effect of solid/liquid interfacial layer (i.e., the interface between the nanoparticle and the fluid) on the thermal conductivity enhancement of nanofluids [32–37].

Yu and Choi [32,33] and Xue and Xu [34] suggested a theoretical model for the effect of a solid/liquid interface based on the Hamilton–Crosser model for suspensions of nano-spherical particles. Their results showed that the solid/liquid interfacial layers play an important role in enhancing the thermal conductivity of nanofluids. Considering the interface effect between the solid particles and the base fluid in nanofluids, Xue [35] developed a model for the effective thermal conductivity of nanofluids based on Maxwell theory and average polarization theory. Xue [35] suggested that the developed model can interpret the anomalous enhancement of the effective thermal conductivity of the nanofluid. On the basis of molecular dynamic simulations and simple liquid–solid interfaces, Xue et al. [37] illustrated that the layering of the liquid atoms at the liquid–solid interface does not have any significant effect on the thermal-transport properties of nanofluids.

Although many possible mechanisms were proposed in the literature, there are no robust theoretical and experimental studies that explain the basis for possible heat-transfer enhancement when using nanofluids. As such, it is still unclear as to what are the best models to use for the thermal conductivity and viscosity of nanofluids. Therefore, the aim of this study is to analyze the variants within the thermophysical characteristics of nanofluids especially with respect to the thermal conductivity and viscosity models and propose possible physical reasons for the deviations between experimental and analytical studies.

2.2 ANALYTICAL MODELS FOR PHYSICAL PROPERTIES OF NANOFLUIDS

2.2.1 Density

The density of nanofluid can be determined analytically based on the physical principle of the mixture rule as

$$\rho_{\text{eff}} = \left(\frac{m}{V}\right)_{\text{eff}} = \frac{m_{\text{f}} + m_{\text{p}}}{V_{\text{f}} + V_{\text{p}}} = \frac{\rho_{\text{f}} V_{\text{f}} + \rho_{\text{p}} V_{\text{p}}}{V_{\text{f}} + V_{\text{p}}} = (1 - \phi_{\text{p}})\rho_{\text{f}} + \phi_{\text{p}}\rho_{\text{p}} \tag{2.1}$$

where f and p refer to the fluid and nanoparticle, respectively, and $\phi_{\text{p}} = (V_{\text{p}}/V_{\text{f}} + V_{\text{p}})$ is the volume fraction of the nanoparticles. To test the validity of Equation 2.1, Pak and Cho [16] and Ho et al. [38] conducted experimental studies to measure the density of Al_2O_3–water nanofluids at room temperature as depicted in Figure 2.1a. Excellent agreement was found between the experimental results and the predictions using Equation 2.1 as shown in Figure 2.1a. Ho et al. [38] also measured the density of Al_2O_3–water nanofluid at different temperatures and nanoparticle volume fractions. Khanafer and Vafai [39] developed a correlation for the density of Al_2O_3–water nanofluid using the experimental data of Ho et al.'s study [38] as a function of temperature and volume fraction of nanoparticles as follows:

$$\rho_{\text{eff}} = 1001.064 + 2738.6191\phi_{\text{p}} - 0.2095T;\ \ 0 \le \phi_{\text{p}} \le 0.04, 5 \le T\,(^{\circ}\text{C}) \le 40 \tag{2.2}$$

The R^2 of the regression is 99.97% and the maximum relative error is 0.22%. It is clear from Figure 2.1b that the present regression (Equation 2.2) is in excellent agreement with the density measurements of Ho et al. [38].

2.2.2 Heat Capacity of Nanofluids

The vast majority of studies on nanofluids have used an analytical model for the specific heat by assuming thermal equilibrium between the nanoparticles and the base fluid phase as follows:

$$\begin{aligned}
(\rho c)_{\text{eff}} &= \rho_{\text{eff}}\left(\frac{Q}{m\Delta T}\right)_{\text{eff}} = \rho_{\text{eff}}\frac{Q_{\text{f}} + Q_{\text{p}}}{(m_{\text{f}} + m_{\text{p}})\Delta T} = \rho_{\text{eff}}\frac{(mc)_{\text{f}}\Delta T + (mc)_{\text{p}}\Delta T}{(m_{\text{f}} + m_{\text{p}})\Delta T} \\
\rightarrow (\rho c)_{\text{eff}} &= \rho_{\text{eff}}\frac{(\rho c)_{\text{f}} V_{\text{f}} + (\rho c)_{\text{p}} V_{\text{p}}}{\rho_{\text{f}} V_{\text{f}} + \rho_{\text{p}} V_{\text{p}}} \\
\Rightarrow c_{\text{eff}} &= \frac{(1 - \phi_{\text{p}})\rho_{\text{f}} c_{\text{f}} + \phi_{\text{p}}\rho_{\text{p}} c_{\text{p}}}{\rho_{\text{eff}}}
\end{aligned} \tag{2.3}$$

where ρ_{p} is the density of the nanoparticle, ρ_{f} is the density of the base fluid, ρ_{eff} is the density of the nanofluid, and c_{p} and c_{f} are the heat capacities of the nanoparticle

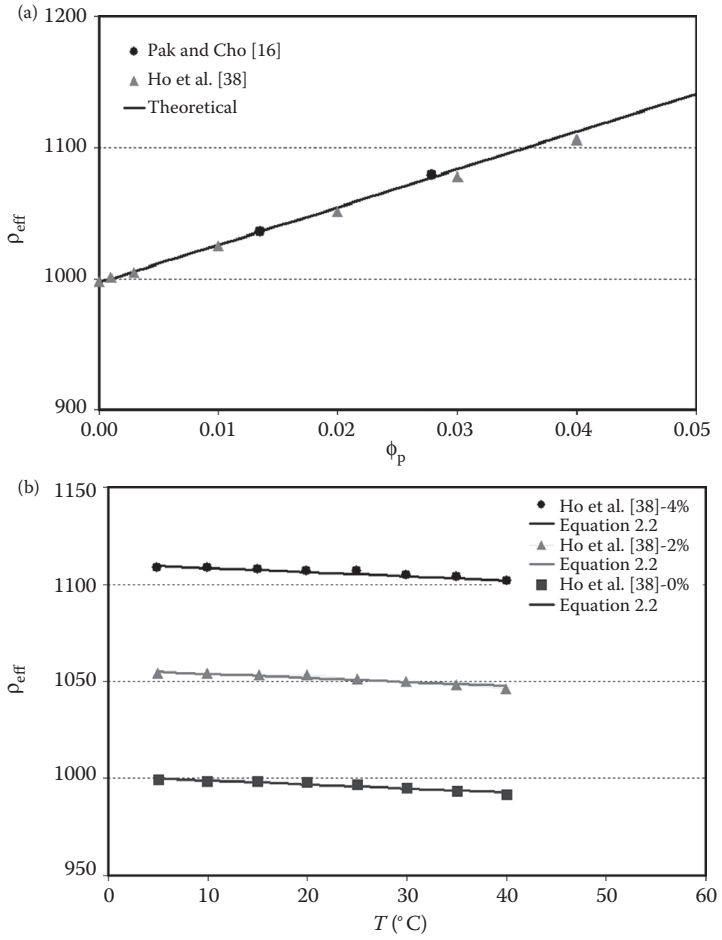

FIGURE 2.1 Effect of the volume fraction on the density of the Al_2O_3–water nanofluid: (a) room temperature; (b) various temperatures. (Reprinted from K. Khanafer and K. Vafai. 2011, A critical synthesis of thermophysical characteristics of nanofluids, *International Journal of Heat and Mass Transfer* 54, 4410–4428, Copyright 2011, with permission from Elsevier.)

and the base fluid, respectively. In contrast, some researchers [16,40–42] suggest a simpler expression given by

$$c_{\text{eff}} = (1 - \phi_p)c_f + \phi_p c_p \tag{2.4}$$

The experimental data of Zhou and Ni [43] were used to evaluate the validity of Equations 2.3 and 2.4, Figure 2.2 shows a comparison of the specific heat of Al_2O_3–water nanofluid at room temperature using both equations with the experimental data of Zhou and Ni [43] for various volume fractions ($\phi_p = 0$–21.7%). Figure 2.2 shows that model I given in Equation 2.3 compares very well with the experimental data of Zhou and Ni [43].

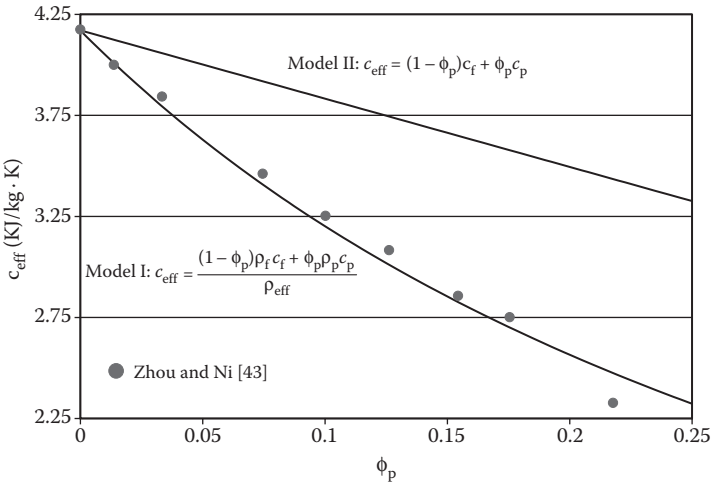

FIGURE 2.2 Comparison of the heat capacity of Al_2O_3–water nanofluid obtained by models I and II given in Equations 2.3 and 2.4 and the experimental data of Zhou and Ni [43]. (Reprinted from K. Khanafer and K. Vafai. 2011, A critical synthesis of thermophysical characteristics of nanofluids, *International Journal of Heat and Mass Transfer* 54, 4410–4428, Copyright 2011, with permission from Elsevier.)

2.2.3 Thermal Expansion Coefficient of Nanofluids

The thermal expansion coefficient of nanofluids can be approximated by utilizing the volume fraction of the nanoparticles on a weight basis as follows [6]:

$$\beta_{eff} = \frac{(1 - \phi_p)(\rho\beta)_f + \phi_p(\rho\beta)_p}{\rho_{eff}} \tag{2.5}$$

where β_f and β_p are the thermal expansion coefficients of the base fluid and the nanoparticle, respectively. However, some investigators give a simpler model for the thermal expansion coefficient of the nanofluid as [44,45]:

$$\beta_{eff} = (1 - \phi_p)\beta_f + \phi_p\beta_p \tag{2.6}$$

Ho et al. [38] conducted an experimental study to estimate the thermal expansion of Al_2O_3–water nanofluid at various volume fractions of nanoparticles. The values of the thermal expansion of Al_2O_3–water nanofluid predicted by Equations 2.5 and 2.6 were compared with the experimental data of Ho et al. [38] at a temperature of 26°C. Figure 2.3a shows that neither Equation 2.5 nor Equation 2.6 can be utilized to correctly determine the thermal expansion of nanofluid as compared with the experimental data of Ho et al. [38]. The effect of varying the temperature and volume fraction of nanoparticles on the thermal expansion coefficient of Al_2O_3–water nanofluid was investigated by Ho et al. [38]. Khanafer and Vafai [39] developed a correlation for the thermal expansion coefficient of Al_2O_3–water nanofluid was developed based

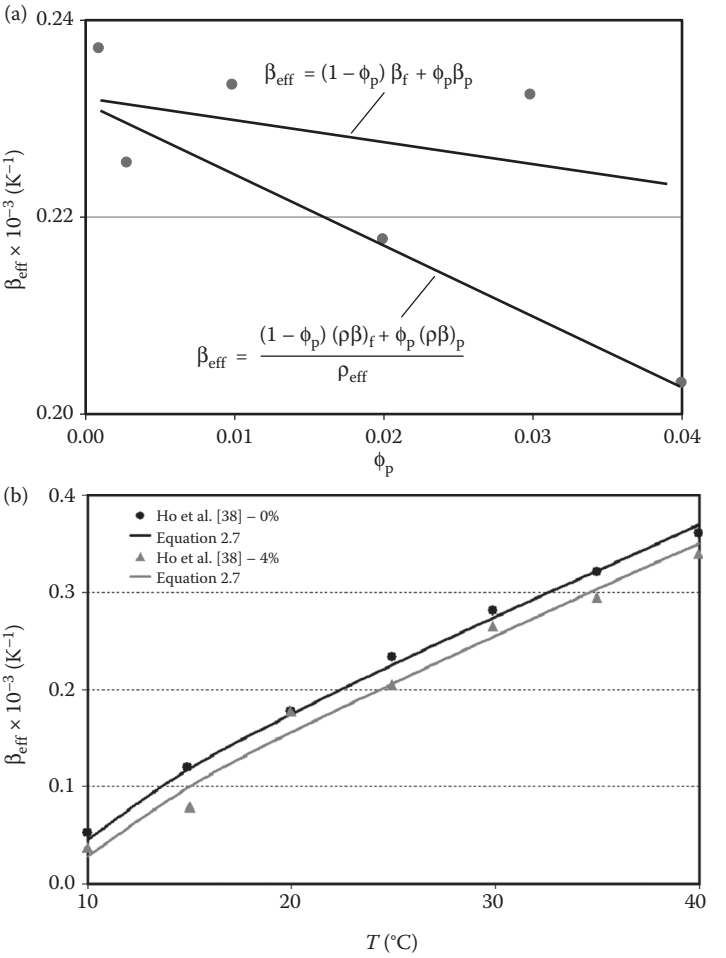

FIGURE 2.3 (a) Effect of volume fraction as displayed by Equations 2.5 and 2.6 at room temperature; (b) temperature effect as displayed by a comparison between Equation 2.7 and experimental data of Ho et al. [38]. (Reprinted from K. Khanafer and K. Vafai. 2011, A critical synthesis of thermophysical characteristics of nanofluids, *International Journal of Heat and Mass Transfer* 54, 4410–4428, Copyright 2011, with permission from Elsevier.)

on the experimental data of Ho et al. [38] as a function of temperature and volume fraction of nanoparticles. This correlation (Al_2O_3–water) can be expressed as [39]:

$$\beta_{eff} = (-0.479\phi_p + 9.3158 \times 10^{-3}T - \frac{4.7211}{T^2}) \times 10^{-3}; \quad 0 \le \phi_p \le 0.04, 10^oC \le T \le 40^oC \tag{2.7}$$

Figure 2.3b shows the validity of the correlation given by Equation 2.7 compared with the experimental data [38].

2.2.4 Effective Viscosity of Nanofluids

2.2.4.1 Analytical Studies

Different analytical models of viscosity have been developed in the literature to model the effective viscosity of nanofluid as a function of volume fraction. Einstein [46] determined the effective viscosity of a suspension of spherical solids as a function of volume fraction (volume concentration <5%) using the phenomenological hydrodynamic equations. This equation was presented as

$$\mu_{\text{eff}} = (1 + 2.5\phi_p)\mu_f \tag{2.8}$$

Since Einstein's model, several equations have been developed in an effort to extend Einstein's formula to suspensions of higher concentrations, including the effect of non-spherical particle concentrations [47–51]. For example, Brinkman [47] presented a viscosity model that extended Einstein's equation to concentrated suspensions:

$$\mu_{\text{eff}} = \frac{1}{(1-\phi_p)^{2.5}} = (1 + 2.5\phi_p + 4.375\phi_p^2 + \cdots)\mu_f \tag{2.9}$$

The effect of Brownian motion on the effective viscosity in a suspension of rigid spherical particles was studied by Batchelor [48]. For isotropic structure of suspension and based on reciprocal theorem in Stokes flow to obtain an expression for the bulk stress, the effective viscosity was given by

$$\mu_{\text{eff}} = (1 + 2.5\phi_p + 6.2\phi_p^2)\mu_f \tag{2.10}$$

Lundgren [49] proposed the following equation under the form of a Taylor series in ϕ_p:

$$\mu_{\text{eff}} = \frac{1}{1-2.5\phi_p}\mu_f = (1 + 2.5\phi_p + 6.25\phi_p^2 + O(\phi_p^3))\mu_f \tag{2.11}$$

It is noticeable that if the terms $O(\phi_p^2)$ and higher are neglected, the above correlation reduces to that of Einstein's model. Table 2.1 summarizes the most common analytical expressions for the viscosity of nanofluids as a function of the volume fraction of the nanoparticles [39].

2.2.4.2 Experimental Studies

A number of experimental studies have been carried out in the literature to determine the dynamic viscosity of nanofluids [16,56–65]. Masuda et al. [57] were the first to measure the dynamic viscosity of several water-based nanofluids for temperatures ranging from room condition to 67°C. Wang et al. [56] obtained some data for the dynamic viscosity of Al_2O_3–water and Al_2O_3–ethylene glycol mixtures at various temperatures.

TABLE 2.1
Summary of Significant Number of Models Found in the Literature

Models	Effective Viscosity	Physical Model	Remarks
Einstein [46]	$\mu_{eff} = (1 + 2.5\phi_p)\mu_f$	Based on the phenomenological hydrodynamic equations Considered a suspension containing n solute particles in a total volume V	Infinitely dilute suspension of spheres (no interaction between the spheres) Valid for relatively low particle volume fraction ($\phi_p \leq 2\%$)
Brinkman [47]	$\mu_{eff} = \frac{1}{(1-\phi_p)^{2.5}}$ $= (1 + 2.5\phi_p + 4.375\phi_p^2 + \cdots)\mu_f$	Based on Einstein model Derived by considering the effect of the addition of one solute molecule to an existing solution	Spherical particles Valid for high-moderate particle concentrations Used Einstein's factor: $(1 + 2.5\phi_p)$
Batchelor [48]	$\mu_{eff} = (1 + \eta\phi_p + k_H\phi_p^2)\mu_f$ $= (1 + 2.5\phi_p + 6.2\phi_p^2)\mu_f$	Based on reciprocal theorem in Stokes flow problem to obtain an expression for the bulk stress due to the thermodynamic forces Incorporated both effects: hydrodynamic effects and Brownian motion	Rigid and spherical particles Brownian motion Isotropic structure Huggins coefficient: $k_H = 6.2$ (5.2 from hydrodynamic effects and 1.0 from Brownian motion)
Lundgren [49]	$\mu_{eff} = \frac{1}{1-2.5\phi_p}\mu_f$ $= (1 + 2.5\phi_p + 6.25\phi_p^2 + \cdots)\mu_f$	Based on a Taylor series expansion in terms of ϕ_p	Dilute concentration of spheres Random bed of spheres
Graham [50]	$\mu_{eff} = (1 + 2.5\phi_p)\mu_f + \left[\frac{4.5}{(h/r_p)(2 + h/r_p)(1 + h/r_p)^2}\right]\mu_f$	A cell theory was used to derive the dependence of the zero-shear-rate viscosity on volume concentration for a suspension of uniform, solid, neutrally buoyant spheres	Agrees well with Einstein's for small ϕ_p r_p is the particle radius and h is the inter-particle spacing

continued

TABLE 2.1 (continued)
Summary of Significant Number of Models Found in the Literature

Models	Effective Viscosity	Physical Model	Remarks
Simha [51]	$\mu_{eff} = \left[1 + 2.5\phi_p + \left(\frac{125}{64\phi_{pmax}}\right)\phi_p^2 + \cdots\right]\mu_f$	Based on Cage model of liquids and solutions	Spherical particles
Mooney [52]	$\mu_{eff} = \exp\left(\frac{2.5\phi_p}{1 - k\phi_p}\right)\mu_f$ $= \left\{1 + 2.5\phi_p + \left[3.125 + (2.5k)\right]\phi_p^2 + \cdots\right\}\mu_f$ $1.35 < k < 1.91$	Einstein's viscosity equation for an infinitely dilute suspension of spheres was extended to apply to a suspension of finite concentration Based on first-order interaction between particles (crowding effect)	Rigid spherical spheres Monodisperse suspension of finite concentration Not valid at high concentrations. Considered the volume fraction of a suspension to be divided into two portions
Eilers [53]	$\mu_{eff} = \mu_f\left[1 + \frac{1.25\phi_p}{1 - \phi_p/0.78}\right]$ $= (1 + 2.5\phi_p + 4.75\phi_p^2 + \cdots)\mu_f$	Based on experimental data	Suspensions of bitumen spheres Curve fitting of the experimental data
Saito [55]	$\mu_{eff} = \left(1 + \frac{2.5}{1 - \phi_p}\phi_p\right)\mu_f$ $= (1 + 2.5\phi_p + 2.5\phi_p^2 + \cdots)\mu_f$	Developed based on a theory for spherical solute-molecules in which a single solute-molecule is placed in the field of flow, obtained by averaging over all the possible positions of a second solute-molecule	Spherical rigid particles Brownian motion Very small particles
Frankel and Acrivos [55]	$\mu_{eff} = \left(\frac{9}{8}\frac{(\phi_p/\phi_{pmax})^{1/3}}{1 - (\phi_p/\phi_{pmax})^{1/3}}\right)\mu_f$	An asymptotic technique was used to derive the functional dependence of effective viscosity on concentration for a suspension of uniform solid spheres, in the limit as concentration approaches its maximum value	Uniform solid particles

Source: Reprinted from K. Khanafer and K. Vafai. 2011, A critical synthesis of thermophysical characteristics of nanofluids, *International Journal of Heat and Mass Transfer* 54, 4410–4428, Copyright 2011, with permission from Elsevier.

Because the formulas such as the one proposed by Einstein [46] and later improved by Brinkman [47] and Batchelor [48] underestimate the viscosity of the nanofluids when compared with the measured data, Maiga et al. [58,59] performed a least-square curve fitting of some experimental data of Wang et al. [56] including Al_2O_3 in water and Al_2O_3 in ethylene glycol. Table 2.2 demonstrates a summary of various dynamic viscosity models at room temperature based on the experimental data.

TABLE 2.2
Summary of Viscosity Models at Room Temperature Based on Experimental Data

Models	Effective Viscosity (Regression)	Remarks
Maiga et al. [58]	$\mu_{eff} = \left(1 + 7.3\phi_p + 123\phi_p^2\right)\mu_f$	Least-square curve fitting of Wang et al. [56] data Al_2O_3–water, $d_p = 28$ nm
Maiga et al. [58]	$\mu_{eff} = \left(1 - 0.19\phi_p + 306\phi_p^2\right)\mu_f$ $d_p = 28\,\text{nm}$	Least-square curve fitting of experimental data [56,57] Al_2O_3–ethylene glycol
Khanafer and Vafai [39]	$\mu_{eff} = \left(1 + 0.164\phi_p + 302.34\phi_p^2\right)\mu_f$ $d_p = 28\,\text{nm}$	Least-square curve fitting of experimental data [55,57] Al_2O_3–ethylene glycol
Buongiorno [66]	$\mu_{eff} = \left(1 + 39.11\phi_p + 533.9\phi_p^2\right)\mu_f$	Curve fitting of Pak and Cho [16] data Al_2O_3–water, $d_p = 13$ nm
Buongiorno [66]	$\mu_{eff} = \left(1 + 5.45\phi_p + 108.2\phi_p^2\right)\mu_f$	Curve fitting of Pak and Cho [16] data TiO_2–water, $d_p = 27$ nm
Khanafer and Vafai [39]	$\mu_{eff} = \left(1 + 23.09\phi_p + 1525.3\phi_p^2\right)\mu_f$ $0 \le \phi_p \le 0.04$	Curve fitting of Pak and Cho [16] data Al_2O_3–water, $d_p = 13$ nm
Khanafer and Vafai [39]	$\mu_{eff} = \left(1 + 3.544\phi_p + 169.46\phi_p^2\right)\mu_f$ $0 \le \phi_p \le 0.1$	Curve fitting of Pak and Cho [16] data TiO_2–water, $d_p = 27$ nm
Nguyen et al. [61]	$\mu_{eff} = \mu_f \times 0.904e^{0.148\phi_p};\ d_p = 47\,\text{nm}$ $\mu_{eff} = \left(1 + 0.025\phi_p + 0.015\phi_p^2\right)\mu_f;\ d_p = 36\,\text{nm}$	Curve fitting of the experimental data Al_2O_3–water
Nguyen et al. [61]	$\mu_{eff} = \left(1.475 - 0.319\phi_p + 0.051\phi_p^2 + 0.009\phi_p^3\right)\mu_f$	Curve fitting of the experimental data CuO–water, $d_p = 29$ nm TiO_2–water Shear rate = 100 s^{-1}
Tseng and Lin [62]	$\mu_{eff} = 13.47 \exp(35.98\phi_p)\ \ \mu_f;\ 0.05 \le \phi_p \le 0.12$	

Source: Reprinted from K. Khanafer and K. Vafai. 2011, A critical synthesis of thermophysical characteristics of nanofluids, *International Journal of Heat and Mass Transfer* 54, 4410–4428, Copyright 2011, with permission from Elsevier.

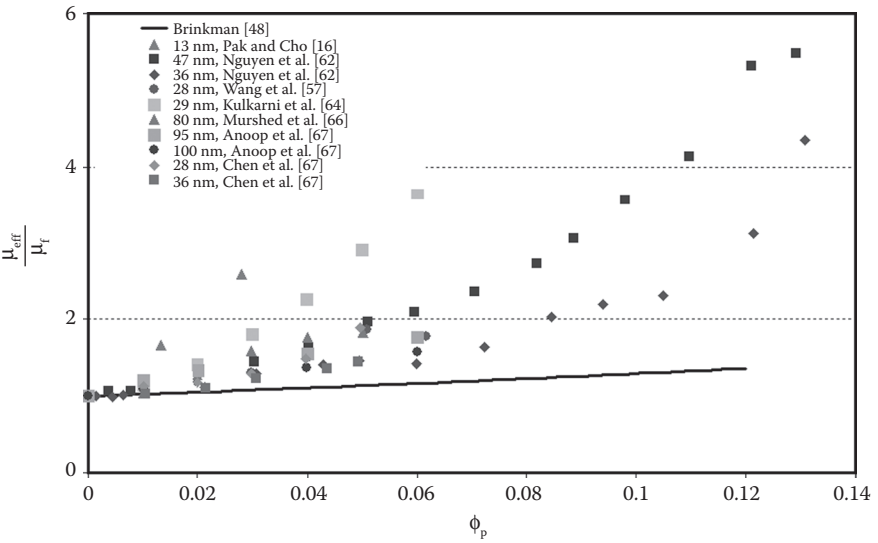

FIGURE 2.4 Relative viscosity measurement as a function of the volume fraction, ϕ_p, at ambient temperature (Al_2O_3–water nanofluid). (Reprinted from K. Khanafer and K. Vafai. 2011, A critical synthesis of thermophysical characteristics of nanofluids, *International Journal of Heat and Mass Transfer* 54, 4410–4428, Copyright 2011, with permission from Elsevier.)

Moreover, Figure 2.4 shows a comparison of the relative dynamic viscosity of Al_2O_3–water nanofluid from various research studies in the literature at room temperature. Figure 2.4 shows that Brinkman model [47], which was derived for two-phase mixture, is to some extent sufficient to estimate the viscosity for relatively low-volume fraction of particles (i.e., $\phi_p \leq 2\%$). Although it noticeably underestimates the nanofluid viscosity when compared with experimental data at high particle concentrations. The differences in the relative viscosity among the experimental data as shown in Figure 2.4 may be due to the difference in the size of the particle clusters, dispersion techniques, and the methods of measurements. This clearly illustrates the discrepancy between the researchers in measuring the dynamic viscosity of nanofluids.

2.3 EFFECT OF TEMPERATURE ON THE DYNAMIC VISCOSITY OF NANOFLUIDS

It should be noted that all the above-mentioned correlations (Tables 2.1 and 2.2) were developed to relate the dynamic viscosity as a function of volume fraction only, without temperature-dependence considerations. Few studies were conducted in the literature on the effect of temperature on the dynamic viscosity of nanofluids [60,61,66–70]. Nguyen et al. [61] analyzed experimentally the effect of temperature on the dynamic viscosities of two water-based nanofluids, namely

Al_2O_3–water ($d_p = 47$ nm, 36 nm) and CuO–water ($d_p = 29$ nm) mixtures. The following correlations were developed by Nguyen et al. [61] for estimating the dynamic viscosity for all nanofluids tested at particle concentrations of 1% and 4%, respectively:

$$\mu_{eff}(cP) = (1.125 - 0.0007 \times T)\mu_f;\ \phi_p = 1\% \tag{2.12}$$

$$\mu_{eff}(cP) = (2.1275 - 0.0215 \times T + 0.0002 \times T^2)\mu_f;\ \phi_p = 4\% \tag{2.13}$$

where T is the temperature in °C. It can be noticed from Equations 2.12 and 2.13 that Nguyen et al. [61] did not explicitly express the dynamic viscosity as a function of temperature and volume fraction. Palm et al. [67] proposed equations for the dynamic viscosity (Pa. s) by means of the polynomial curve fitting based on the data reported by Putra et al. [13]. The resulting equations as a function of temperature, expressed in Kelvin, for Al_2O_3–water are:

$$\mu_{eff} = 0.034 - 2 \times 10^{-4} T + 2.9 \times 10^{-7} T^2, \phi_p = 1\% \tag{2.14}$$

$$\mu_{eff} = 0.039 - 2.3 \times 10^{-4} T + 3.4 \times 10^{-7} T^2, \phi_p = 4\% \tag{2.15}$$

Tables 2.3 and 2.4 present a summary of different models of the dynamic viscosity of nanofluids as a function of temperature and volume fraction of nanoparticles. Khanafer and Vafai [39] developed a general correlation (Equation 2.16) for the effective viscosity of Al_2O_3–water using various experimental data found in the literature (Figure 2.5a) as a function of volume fraction, nanoparticles diameter, and temperature as follows:

$$\begin{aligned}\mu_{eff}(cP) = &-0.4491 + \frac{28.837}{T} + 0.574\phi_p - 0.1634\phi_p^2 + 23.053\frac{\phi_p^2}{T^2} \\ &+0.0132\phi_p^3 - 2354.735\frac{\phi_p}{T^3} + 23.498\frac{\phi_p^2}{d_p^2} - 3.0185\frac{\phi_p^3}{d_p^2}; \\ &1\% \le \phi_p \le 9\%, 20 \le T(^\circ\mathrm{C}) \le 70, 13\,\mathrm{nm} \le d_p \le 131\,\mathrm{nm}\end{aligned} \tag{2.16}$$

The validity of the above correlation (Equation 2.16) is shown in Figure 2.5b. As can be noticed in Figure 2.5a, the viscosity of the nanofluid decreases with an increase in the temperature. Moreover, there is no agreement between researchers about the experimentally measured values of the nanofluid's viscosity. Published results indicate a surprising range of variation of the results.

TABLE 2.3
Effect of Temperature and Volume Fraction on the Dynamic Viscosity of Nanofluids (Al_2O_3–Water)

Reference	Model (Regression)	Remarks
Khanafer and Vafai [39]	$\mu_{eff} = 0.444 - 0.254\phi_p + 0.0368\phi_p^2 + 26.333\frac{\phi_p}{T} - 59.311\frac{\phi_p^2}{T^2}$ $20 \le T(^\circ\text{C}) \le 70;\ \phi_p = 1.34\%,\ 2.78\%$	Curve fitting of Pak and Cho [16] data $d_p = 13$ nm Units: mPa.s
Palm et al. [67]	$\mu_{eff} = 0.034 - 2\times10^{-4}T(\text{K}) + 2.9\times10^{-7}T^2(\text{K}),\ \phi_p = 1\%$ $\mu_{eff} = 0.039 - 2.3\times10^{-4}T(\text{K}) + 3.4\times10^{-7}T^2(\text{K}),\ \phi_p = 4\%$	Curve fitting of the experimental data, Putra et al. [13] $d_p = 131.2$ nm Units: Pa.s Units: mPa.s
Nguyen et al. [61]	$\mu_{eff} = (1.125 - 0.0007\times T(^\circ\text{C}))\mu_f;\ \phi_p = 1\%$ $\mu_{eff} = (2.1275 - 0.0215\times T(^\circ\text{C}) + 0.0002\times T^2(^\circ\text{C}))\mu_f;\ \phi_p = 4\%$	
Khanafer and Vafai [39]	$\mu_{eff} = -0.4892 + \frac{26.9036}{T} + 0.6837\phi_p + \frac{24.1141}{T^2} - 0.1785\phi_p^2 + 0.1818\frac{\phi_p}{T} + 27.015\frac{\phi_p^2}{T^2}$ $+0.0132\phi_p^3 - 2940.1775\frac{\phi_p}{T^3};\quad 1\% \le \phi_p \le 9.4\%, 20 \le T(^\circ\text{C}) \le 70$	Curve fitting of Nguyen et al. [61] data $d_p = 47$ nm Units: mPa.s
Khanafer and Vafai [39]	$\mu_{eff} = -0.1011 + \frac{18.0162}{T} + 0.3619\varphi_p + \frac{164.0837}{T^2} - 0.0966\varphi_p^2 + 0.1609\frac{\phi_p}{T} + 22.4901\frac{\phi_p^2}{T^2}$ $+0.0078089\varphi_p^3 - 2316.3754\frac{\phi_p}{T^3};\quad 1\% \le \phi_p \le 9.1\%, 20 \le T(^\circ\text{C}) \le 70$	Curve fitting of Nguyen et al. [61] data $d_p = 36$ nm Units: mPa.s
Khanafer and Vafai [39]	$\mu_{eff} = -0.4491 + \frac{28.837}{T} + 0.574\phi_p - 0.1634\phi_p^2 + 23.053\frac{\phi_p^2}{T^2} + 0.0132\phi_p^3 - 2354.735\frac{\phi_p}{T^3}$ $+23.498\frac{\phi_p^2}{d_p^2} - 3.0185\frac{\phi_p^3}{d_p^2};\quad 1\% \le \phi_p \le 9\%, 20 \le T(^\circ\text{C}) \le 70, 13\,\text{nm} \le d_p \le 131\,\text{nm}$	Curve fitting of various experimental data available in the literature [13,16,61,71] Units: mPa.s
Namburu et al. [69,60]	$\text{Log}(\mu_{eff}) = Ae^{-\text{BT}}, \text{in mmPa.s}$ $A = -0.29956\phi_p^3 + 6.7388\phi_p^2 - 55.444\phi_p + 236.11$ $B = (-6.4745\phi_p^3 + 140.03\phi_p^2 - 1478.5\phi_p + 20341)/10^6$	Experimental Al_2O_3–ethylene glycol and water mixture $1\% \le \phi_p \le 10\%$, $d_p = 53$ nm $238 < T < 323\ K$

Source: Reprinted from K. Khanafer and K. Vafai. 2011, A critical synthesis of thermophysical characteristics of nanofluids, *International Journal of Heat and Mass Transfer* 54, 4410–4428, Copyright 2011, with permission from Elsevier.

TABLE 2.4
Effect of Temperature and Volume Fraction on the Dynamic Viscosity of Nanofluids (TiO_2–Water, CuO–Water)

Models	Effective Viscosity (Regression)	Remarks
Duangthongsuk and Wongwises [68]	$\frac{\mu_{eff}}{\mu_f} = 1.0226 + 0.0477\phi_p - 0.0112\phi_p^2;\ T = 15°C$ $\frac{\mu_{eff}}{\mu_f} = 1.013 + 0.092\phi_p - 0.015\phi_p^2;\ T = 25°C$ $\frac{\mu_{eff}}{\mu_f} = 1.018 + 0.112\phi_p - 0.0177\phi_p^2;\ T = 35°C$	Experimental data TiO_2–Water, $0.2 \le \phi_p \le 2\%$ $d_p = 21$ nm
Khanafer and Vafai [39]	$\frac{\mu_{eff}}{\mu_f} = 1.0538 + 0.1448\phi_p - 3.363\times10^{-3}T - 0.0147\phi_p + 6.735\times10^{-5}T^2 - 1.337\frac{\phi_p}{T}$ $15°C \le T \le 35°C, 0.2\% \le \phi_p \le 2\%$	Curve fitting of the experimental data [68] TiO_2–water $d_p = 21$ nm
Khanafer and Vafai [39]	$\mu_{eff} = 0.6002 - 0.569\phi_p + 0.0823\phi_p^2 + 28.8763\frac{\phi_p}{T} - 204.2202\frac{\phi_p^2}{T^2} + 561.3175\frac{\phi_p^3}{T^3}$ $20 \le T(°C) \le 70;\quad \phi_p = 0.99\%,\ 2.04\%,\ 3.16\%$	Curve fitting of Pak and Cho [16] data TiO_2–water $d_p = 27$ nm Units: mmPa.s
Khanafer and Vafai [39]	$\mu_{eff} = -0.4262 + \frac{8.4312}{T} + 0.898\phi_p + \frac{524.7147}{T^2} - 0.2217\phi_p^2 - 4.7329\frac{\phi_p}{T} + 70.3105\frac{\phi_p^2}{T^2}$ $+ 0.0176\phi_p^3 - 5559.4641\frac{\phi_p}{T^3};\quad 1\% \le \phi_p \le 9\%,\ 20 \le T(°C) \le 70$	Curve fitting of Nguyen et al. [59] data CuO–water $d_p = 29$ nm Units: mmPs.s
Namburu et al. [60]	$\mathrm{Log}(\mu_{eff}) = Ae^{-BT},$ in mm Pa.s $A = 1.8375\phi_p^2 - 29.643\phi_p + 165.56$ $B = 4\times10^{-6}\phi_p^2 - 0.001\phi_p + 0.0186$	CuO–ethylene glycol and water mixture $1 \le \phi_p \le 6\%$, $d_p = 29$ nm $238 < T < 323$ K

continued

TABLE 2.4 (continued)
Effect of Temperature and Volume Fraction on the Dynamic Viscosity of Nanofluids (TiO_2–Water, CuO–Water)

Models	Effective Viscosity (Regression)	Remarks
Kulkarni et al. [63,64]	$\ln \mu_{eff} = A\left(\frac{1}{T}\right) - B$, in mm Pa.s $A = 20587\phi_p^2 + 15857\phi_p + 1078.3$ $B = -107.12\phi_p^2 + 53.54\phi_p + 2.8715$	CuO–water. $0.05 \le \phi_p \le 0.15$ $d_p = 29$ nm. $278 \le T \le 323$ K Shear rate = 100 1/s
Koo and Kleinstreuer [70]	$\mu_{eff} = \mu_{static} + \mu_{Brownian}$ $\mu_{Brownian} = 5 \times 10^4 \beta \rho_f \phi_p \sqrt{\frac{\kappa T}{\rho_p d_p}} f(\varphi_p, T)$ $f(\phi_p, T) = (-6.04\phi + 0.4705)T + (1722.3\phi_p - 134.63)$ $\beta = \begin{cases} 0.0137(100\phi_p)^{-0.8229}, & \phi_p < 0.01 \\ 0.0011(100\phi_p)^{-0.7272}, & \phi_p > 0.01 \end{cases}$ $1\% < \phi_p < 4\%,\ 300 < T < 325$K	CuO–water

Source: Reprinted from K. Khanafer and K. Vafai. 2011, A critical synthesis of thermophysical characteristics of nanofluids, *International Journal of Heat and Mass Transfer* 54, 4410–4428, Copyright 2011, with permission from Elsevier.

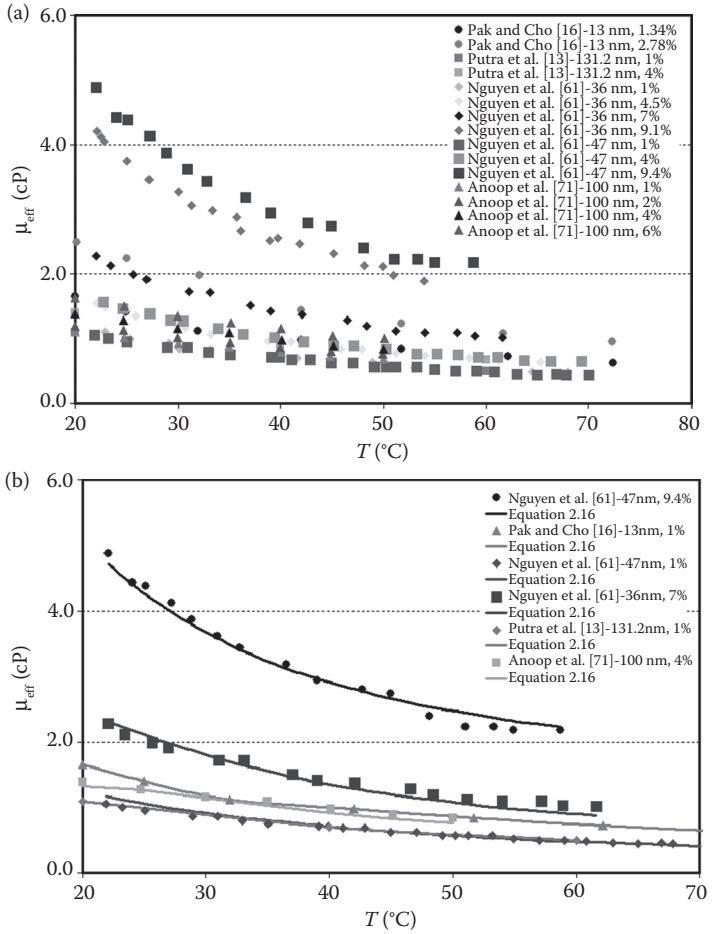

FIGURE 2.5 Effect of the volume fraction and temperature on the effective viscosity of Al_2O_3–water nanofluid: (a) experimental measurements; (b) comparison of Equation 2.16 developed in the current work with the experimental data. (Reprinted from K. Khanafer and K. Vafai. 2011, A critical synthesis of thermophysical characteristics of nanofluids, *International Journal of Heat and Mass Transfer* 54, 4410–4428, Copyright 2011, with permission from Elsevier.)

2.4 THERMAL CONDUCTIVITY OF NANOFLUIDS

Several experimental and theoretical studies were reported in the literature with respect to modeling thermal conductivity of nanofluids. The published results are in disagreement regarding the mechanisms for heat-transfer enhancement as well as a cohesive possible clarification with respect to the large discrepancies in the results even for the same base fluid and nanoparticles size. At present, there are no theoretical results available in the literature that can accurately determine the thermal conductivity of nanofluids. The existing results were generally based on

the definition of the effective thermal conductivity of a two-component mixture as follows [72]:

$$k_{\text{eff}} = \frac{k_{\text{f}}(1-\phi_{\text{p}})(\mathrm{d}T/\mathrm{d}x)_{\text{f}} + k_{\text{p}}\phi_{\text{p}}(\mathrm{d}T/\mathrm{d}x)_{\text{p}}}{\phi_{\text{p}}(\mathrm{d}T/\mathrm{d}x)_{\text{p}} + (1-\phi_{\text{p}})(\mathrm{d}T/\mathrm{d}x)_{\text{f}}} \tag{2.17}$$

where $(\mathrm{d}T/\mathrm{d}x)_{\text{f}}$ is the temperature gradient within the fluid and $(\mathrm{d}T/\mathrm{d}x)_{\text{p}}$ is the temperature gradient through the particle. The Maxwell model [73] was one the first models developed for solid–liquid mixture with relatively large particles based on the solution of heat-conduction equation through a stationary random suspension of spheres. The effective thermal conductivity is given by

$$k_{\text{eff}} = \frac{k_{\text{p}} + 2k_{\text{f}} + 2\phi_{\text{p}}(k_{\text{p}} - k_{\text{f}})}{k_{\text{p}} + 2k_{\text{f}} - \phi_{\text{p}}(k_{\text{p}} - k_{\text{f}})}k_{\text{f}} = k_{\text{f}} + \frac{3\phi_{\text{p}}(k_{\text{p}} - k_{\text{f}})}{k_{\text{p}} + 2k_{\text{f}} - \phi_{\text{p}}(kp - k_{\text{f}})} \tag{2.18}$$

where k_{p} is the thermal conductivity of the particles, k_{f} is the fluid thermal conductivity, and ϕ_{p} is the volume fraction of the suspended particles. The Maxwell model is precise to the order of φ_{p}^{1} and applicable for the range of $\phi_{\text{p}} \ll 1$ or $|(k_{\text{p}}/k_{\text{f}}) - 1| \ll 1$, Bruggeman [74] developed a model to study the interactions between randomly dispersed spherical particles as follows:

$$\begin{aligned} \frac{k_{\text{eff}}}{k_{\text{f}}} &= \frac{(3\phi_{\text{p}} - 1)(k_{\text{p}}/k_{\text{f}}) + \left\{3(1-\phi_{\text{p}}) - 1\right\} + \sqrt{\Delta}}{4}; \\ \Delta &= \left[(3\phi_{\text{p}} - 1)\frac{k_{\text{p}}}{k_{\text{f}}} + \left\{3(1-\phi_{\text{p}}) - 1\right\}\right]^2 + 8\frac{k_{\text{p}}}{k_{\text{f}}} \end{aligned} \tag{2.19}$$

The Bruggeman model [74] is applicable for large volume fraction of spherical particles. For low-volume fractions, the Bruggeman model [74] results reduce to the Maxwell model [73]. For non-spherical particles, Hamilton and Crosser [72] proposed a model for the effective thermal conductivity of two-component mixtures as a function of the thermal conductivity of both the base fluid and the particle, volume fraction of the particles, and the shape of the particles. For the thermal conductivity ratio of two phases larger than 100 ($k_{\text{p}}/k_{\text{f}} > 100$), the thermal conductivity of two-component mixtures can be expressed as follows [72]:

$$k_{\text{eff}} = \frac{k_{\text{p}} + (n-1)k_{\text{f}} + (n-1)\phi_{\text{p}}(k_{\text{p}} - k_{\text{f}})}{k_{\text{p}} + (n-1)k_{\text{f}} - \phi_{\text{p}}(k_{\text{p}} - k_{\text{f}})}k_{\text{f}} \tag{2.20}$$

where n is the empirical shape factor given by $n = 3/\psi$, and ψ is the particle sphericity, defined by the ratio of the surface area of a sphere with volume equal to that of the particle, to the surface area of the particle. Tables 2.5 through 2.7 review some relevant models for the effective thermal conductivity of nanofluids including the effects of Brownian motion and the nano-layer.

TABLE 2.5
Summary of Theoretical Models for the Effective Thermal Conductivity of Nanofluids

Models	Expressions	Physical Model	Remarks
Maxwell [73]	$\frac{k_{\text{eff}}}{k_{\text{f}}} = \frac{k_{\text{p}} + 2k_{\text{f}} + 2\phi_{\text{p}}(k_{\text{p}} - k_{\text{f}})}{k_{\text{p}} + 2k_{\text{f}} - \phi_{\text{p}}(k_{\text{p}} - k_{\text{f}})}$	Based on the conduction solution through a stationary random suspension of spheres	Spherical particles Accurate to order φ_{p}^{1}.
Bruggeman [74]	$\frac{k_{\text{eff}}}{k_{\text{f}}} = \frac{(3\phi_{\text{p}} - 1)k_{\text{p}}/k_{\text{f}} + \left\{3(1-\phi_{\text{p}}) - 1\right\} + \sqrt{\Delta}}{4}$ $\Delta = \left[(3\phi_{\text{p}} - 1)\frac{k_{\text{p}}}{k_{\text{f}}} + \left\{3(1-\phi_{\text{p}}) - 1\right\}\right]^2 + 8\frac{k_{\text{p}}}{k_{\text{f}}}$	Based on the differential effective medium theory to estimate the effective thermal conductivity of composites at high particle concentrations It consists in building up the composite medium through a process of incremental homogenization	Applicable to high-volume fraction of spherical particles Suspension with spherical inclusions. No shape factor
Hamilton and Crosser [72]	$\frac{k_{\text{eff}}}{k_{\text{f}}} = \frac{k_{\text{p}} + (n-1)k_{\text{f}} + (n-1)\phi_{\text{p}}(k_{\text{p}} - k_{\text{f}})}{k_{\text{p}} + (n-1)k_{\text{f}} - \phi_{\text{p}}(k_{\text{p}} - k_{\text{f}})}$	Based on the effective thermal conductivity of a two-component mixture	Spherical and non-spherical particles. $n = 3$ (spheres), $n = 6$ (cylinders)
Wasp [75]	$\frac{k_{\text{eff}}}{k_{\text{f}}} = \frac{k_{\text{p}} + 2k_{\text{f}} + 2\phi_{\text{p}}(k_{\text{p}} - k_{\text{f}})}{k_{\text{p}} + 2k_{\text{f}} - \phi_{\text{p}}(k_{\text{p}} - k_{\text{f}})}$	Based on effective thermal conductivity of a two-component mixture	Special case of Hamilton and Crosser's model with $n = 3$
Jeffery [76]	$\frac{k_{\text{eff}}}{k_{\text{f}}} = 1 + 3\eta\phi_{\text{p}} + \phi_{\text{p}}^2\left(3\eta^2 + \frac{3\eta^2}{4} + \frac{9\eta^3}{16}\frac{\kappa+2}{2\kappa+3} + \cdots\right)$ $\kappa = \frac{k_{\text{p}}}{k_{\text{f}}}, \eta = \frac{\kappa - 1}{\kappa + 2}$	Based on the conduction solution through a stationary random suspension of spheres	High order terms represent pair interactions of randomly dispersed spherical particles Accurate to order φ_{p}^2

continued

TABLE 2.5 (continued)
Summary of Theoretical Models for the Effective Thermal Conductivity of Nanofluids

Models	Expressions	Physical Model	Remarks
Davis [77]	$\frac{k_{\text{eff}}}{k_{\text{f}}} = 1 + \frac{3(\kappa - 1)}{(\kappa + 2) - \phi_{\text{p}}(\kappa - 1)}\left[\phi_{\text{p}} + f(\kappa)\phi_{\text{p}}^2 + O(\phi_{\text{p}}^3)\right]$ $\kappa = \frac{k_{\text{p}}}{k_{\text{f}}}$	Green's theorem was applied to the space occupied by the matrix material (spherical inclusions) Decaying temperature field was used	Accurate to order φ_{p}^2 High-order terms represent pair interactions of randomly dispersed particles $f(\kappa) = 2.5$ for $\kappa = 10$ $f(\kappa) = 0.5$ for $\kappa = \infty$
Lu and Lin [78]	$\frac{k_{\text{eff}}}{k_{\text{f}}} = 1 + a\phi_{\text{p}} + b\phi_{\text{p}}^2$	The effective conductivity of composites containing aligned spheroids of finite conductivity was modeled with the pair interaction The pair interaction was evaluated by solving a boundary value problem involving two aligned spheroids	Spherical and non-spherical particles. Spherical particles: $a = 2.25$, $b = 2.27$ for $\kappa = 10$; $a = 3$, $b = 4.51$ for $\kappa = \infty$

Source: Reprinted from K. Khanafer and K. Vafai. 2011, A critical synthesis of thermophysical characteristics of nanofluids, *International Journal of Heat and Mass Transfer* 54, 4410–4428, Copyright 2011, with permission from Elsevier.

TABLE 2.6
Summary of Theoretical Models for the Effective Thermal Conductivity of Nanofluids (Nano-Layer Effect)

Models	Expressions	Physical Model	Remarks
Yu and Choi [32]	$k_{\text{eff}} = \dfrac{k_{\text{pe}} + 2k_{\text{f}} + 2\phi_{\text{p}}(k_{\text{pe}} - k_{\text{f}})(1+\beta)^3}{k_{\text{pe}} + 2k_{\text{f}} - \phi_{\text{p}}(k_{\text{pe}} - k_{\text{f}})(1+\beta)^3} k_{\text{f}}$ $k_{\text{pe}} = \dfrac{2(1-\gamma) + (1+\beta)^3(1+2\gamma)\gamma}{-(1-\gamma) + (1+\beta)^3(1+2\gamma)} k_{\text{p}}$ $\beta = t/r_{\text{p}}$ and $\gamma = k_{\text{layer}}/k_{\text{p}}$	Modified Maxwell model [73]	Spherical particles Nano-layer
Yu and Choi [33]	$k_{\text{eff}} = \left(1 + \dfrac{nf_e A}{1 - f_e A}\right) k_{\text{f}}$ $A = \dfrac{1}{3} \sum_{j=a,b,c} \dfrac{(k_{\text{p}j} - k_{\text{f}})}{k_{\text{p}j} + (n-1)k_{\text{f}}}$ $f_e = \dfrac{f\sqrt{(a^2+t)(b^2+t)(c^2+t)}}{\text{abc}}$	Modified Hamilton–Crosser model [72]	Nonspherical particles. Nano-layer
Xue [35]	$9\left(1 - \dfrac{\phi_{\text{p}}}{\lambda}\right) \dfrac{k_{\text{eff}} - k_{\text{f}}}{2k_{\text{eff}} + k_{\text{f}}} + \dfrac{\phi_{\text{p}}}{\lambda} \dfrac{k_{\text{eff}} - k_{c,x}}{k_{\text{eff}} + B_{2,x}(k_{c,x} - k_{\text{eff}})}$ $+ \dfrac{\phi_{\text{p}}}{\lambda} 4 \dfrac{k_{\text{eff}} - k_{c,y}}{2k_{\text{eff}} + (1 - B_{2,x})(k_{c,y} - k_{\text{eff}})} = 0$	Based on the Maxwell model and the average polarization theory and on the assumption that there is an interfacial shell between the nanoparticles and the base fluid	Spherical particles Nano-layer

continued

TABLE 2.6 (continued)
Summary of Theoretical Models for the Effective Thermal Conductivity of Nanofluids (Nano-Layer Effect)

Models	Expressions	Physical Model	Remarks
Xue and Xu [34]	$\left(1-\frac{\phi_p}{\kappa}\right)\frac{k_{eff}-k_f}{2k_{eff}+k_f}$ $+\frac{\phi_p}{\kappa}\frac{(k_{eff}-k_{shell})(2k_{shell}+k_p)-\kappa(k_p-k_{shell})(2k_{shell}+k_{eff})}{(2k_{eff}+k_{shell})(2k_{shell}+k_p)+2\kappa(k_p-k_{shell})(k_{shell}-k_{eff})}=0$	A modified Bruggeman model [74] including the effect of interfacial shells	Spherical particles Nano-layer
Xie et al. [36]	$\frac{k_{eff}-k_f}{k_f}=3\Theta\phi_T+\frac{3\Theta^2\phi_T^2}{1-\Theta\phi_T}$ $\phi_T=\frac{4}{3}\pi(r_p+t)^3N_p=\phi_p(1+\beta)^3,\ \beta=\frac{t}{r_p}$	Based on Fourier's law of heat conduction	Low particle loadings Nano-layer

Source: Reprinted from K. Khanafer and K. Vafai. 2011, A critical synthesis of thermophysical characteristics of nanofluids, *International Journal of Heat and Mass Transfer* 54, 4410–4428, Copyright 2011, with permission from Elsevier.

TABLE 2.7
Summary of Theoretical Models for the Effective Thermal Conductivity of Nanofluids (Brownian Effect)

Models	Expressions	Physical Model	Remarks
Wang et al. [19]	$\frac{k_{\text{eff}}}{k_{\text{f}}} = \frac{(1-\phi_{\text{p}}) + 3\phi_{\text{p}}\int_0^\infty (k_{cl}(r)n(r)/k_{cl}(r) + 2k_{\text{f}})\,\text{d}r}{(1-\phi_{\text{p}}) + 3\phi_{\text{p}}\int_0^\infty (k_{\text{f}}(r)n(r)/k_{cl}(r) + 2k_{\text{f}})\,\text{d}r}$	Based on the effective medium approximation and the fractal theory for predicting the thermal conductivity of nanofluids	Accounts for the size effect and the surface adsorption of nanoparticles
Xuan et al. [79]	$\frac{k_{\text{eff}}}{k_{\text{f}}} = \frac{k_{\text{p}} + 2k_{\text{f}} - 2\phi_{\text{p}}(k_{\text{f}} - k_{\text{p}})}{k_{\text{p}} + 2k_{\text{f}} + \phi_{\text{p}}(k_{\text{f}} - k_{\text{p}})} + \frac{\rho_{\text{p}}\phi_{\text{p}}c_{\text{p}}}{2k_{\text{f}}}\sqrt{\frac{k_B T}{3\pi r_c \mu}}$	Based on Maxwell model The theory of Brownian motion and the diffusion-limited aggregation model are applied to simulate random motion and the aggregation process of the nanoparticles	Includes the effect of random motion, particle size, concentration, and temperature
Jang and Choi [10]	$k_{\text{eff}} = k_{\text{f}}(1-\phi_{\text{p}}) + k_{\text{p}}\phi_{\text{p}} + 3C\frac{d_{\text{f}}}{d_{\text{p}}}k_{\text{f}}\,\text{Re}_{d_{\text{p}}}^2\,\text{Pr}\,\phi_{\text{p}}$	A theoretical model was developed based on kinetics, Kapitza resistance, and convection A general expression for the thermal conductivity of nanofluids involving four modes of energy transport in nanofluids was derived	Considered four modes of energy transport: collision between fluid molecules, thermal diffusion of nanoparticles, collision between nanoparticles due to Brownian motion, and thermal interactions of dynamic nanoparticles with fluid molecules Collision of nanoparticles due to Brownian motion is neglected
Prasher et al. [80]	$k_{\text{eff}} = (1 + A\,\text{Re}^m\,\text{Pr}^{0.333}\,\phi_{\text{p}}) \times \left[\frac{k_{\text{p}} + 2k_{\text{f}} + 2\phi_{\text{p}}(k_{\text{p}} - k}{k_{\text{p}} + 2k_{\text{f}} - \phi_{\text{p}}(k_{\text{p}} - k_{\text{f}}}\right.$	Based on Maxwell model and heat transfer in fluidized beds	Accounts for convection caused by the Brownian motion from multiple nanoparticles

continued

TABLE 2.7 (continued)
Summary of Theoretical Models for the Effective Thermal Conductivity of Nanofluids (Brownian Effect)

Models	Expressions	Physical Model	Remarks
Koo and Kleinstreuer [70,81]	$k_{\text{eff}} = k_{\text{static}} + k_{\text{Brownian}} = \dfrac{k_p + 2k_f + 2\phi_p(k_p - k_f)}{k_p + 2k_f - \phi_p(k_p - k_f)} k_f + 5 \times 10^4 \beta \phi_p \rho_p c_p \sqrt{\dfrac{k_B T}{\rho_p D}} f(T, \phi_p)$	Based on Maxwell model Curve fitting of the available experimental data to determine the effective conductivity due to Brownian motion	Considered surrounding liquid traveling with randomly moving nanoparticles
Chon et al. [82]	$\dfrac{k_{\text{eff}}}{k_f} = 1 + 64.7\phi_p^{0.74}\left(\dfrac{d_f}{d_p}\right)^{0.369}\left(\dfrac{k_p}{k_f}\right)^{0.747} \times \text{Pr}^{0.9955}\,\text{Re}^{1.2321}$ $\text{Pr} = \dfrac{\mu_f}{\rho_f \alpha_f}$, $\text{Re} = \dfrac{\rho_f V_{Br} d_p}{\mu_f} = \dfrac{\rho_f k_B T}{3\pi\mu_f^2 l_f}$	Based on the curve fitting of the experimental data	Reynolds number is based on the Brownian motion velocity

Source: Reprinted from K. Khanafer and K. Vafai. 2011, A critical synthesis of thermophysical characteristics of nanofluids, *International Journal of Heat and Mass Transfer* 54, 4410–4428, Copyright 2011, with permission from Elsevier.

2.4.1 Experimental Investigations

Many studies have reported augmentation in the effective thermal conductivity of nanofluids at room temperature. Figures 2.6a and 2.6b illustrate the effective thermal conductivity measurements at ambient temperature for Al_2O_3–water and CuO–water nanofluids at various volume concentrations and nanoparticle diameters. Figure 2.6 shows that the effective thermal conductivity of nanofluids increases with an increase in the volume fraction of nanoparticles. In addition, the size of the particles is found to have a substantial effect on the thermal conductivity improvement. It should be noted that smaller particles exhibit larger surface area-to-volume ratio than the larger particles. As such, smaller particle diameters can possibly result in a

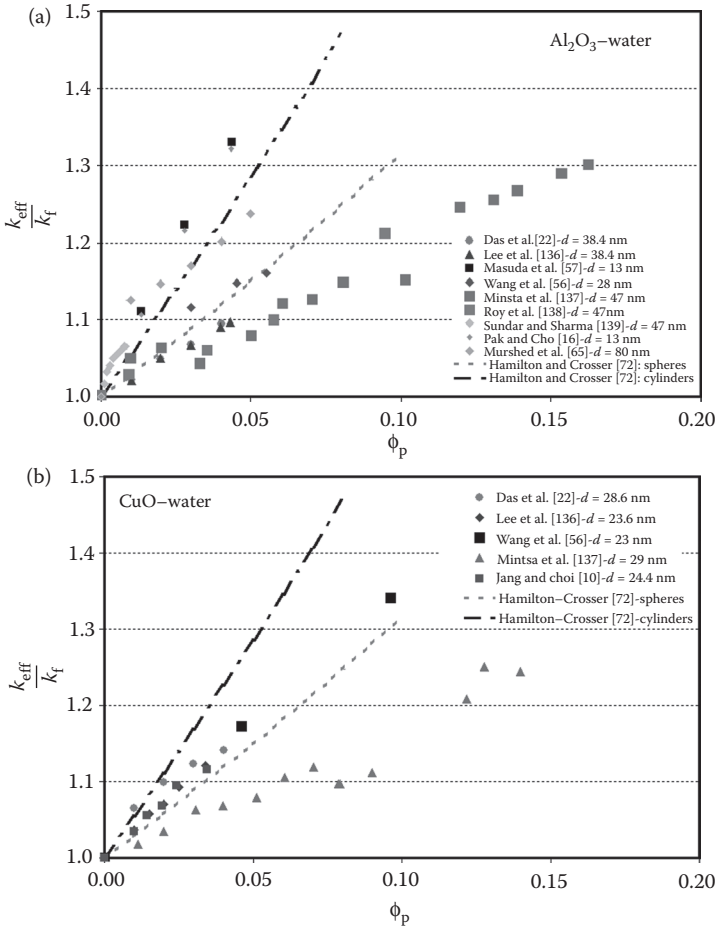

FIGURE 2.6 Effect of the volume fraction on the effective thermal conductivity measurements: (a) Al_2O_3–water; (b) CuO–water. (Reprinted from K. Khanafer and K. Vafai. 2011, A critical synthesis of thermophysical characteristics of nanofluids, *International Journal of Heat and Mass Transfer* 54, 4410–4428, Copyright 2011, with permission from Elsevier.)

larger augmentation in the effective thermal conductivity of nanofluids. It is interesting to note from Figures 2.6a and 2.6b that the Hamilton and Crosser model [72] may represent a good approximation for the effective thermal conductivity value for smaller volume fractions ($\phi_p \leq 4\%$).

A general correlation for the effective thermal conductivity of Al_2O_3–water and CuO–water nanofluids at ambient temperature accounting for various volume fractions and nanoparticles diameters was developed by Khanafer and Vafai [39] using various experimental data. This model was expressed as

$$\frac{k_{\text{eff}}}{k_f} = 1.0 + 1.0112\phi_p + 2.4375\phi_p\left(\frac{47}{d_p(\text{nm})}\right) - 0.0248\phi_p\left(\frac{k_p}{0.613}\right); \quad R^2 = 96.5\% \tag{2.21}$$

where k_f is the thermal conductivity of water. Figure 2.7 demonstrates that the general correlation, represented by Equation 2.21, is in good agreement with the experimental measurements of Al_2O_3–water and CuO–water nanofluids.

Thermal conductivity measurements at different temperatures are important because the measurements at ambient temperature are not sufficient for estimating the heat transfer characteristics of nanofluids. Figure 2.8 shows a comparison of the relative effective thermal conductivity (ratio of the effective thermal conductivity of

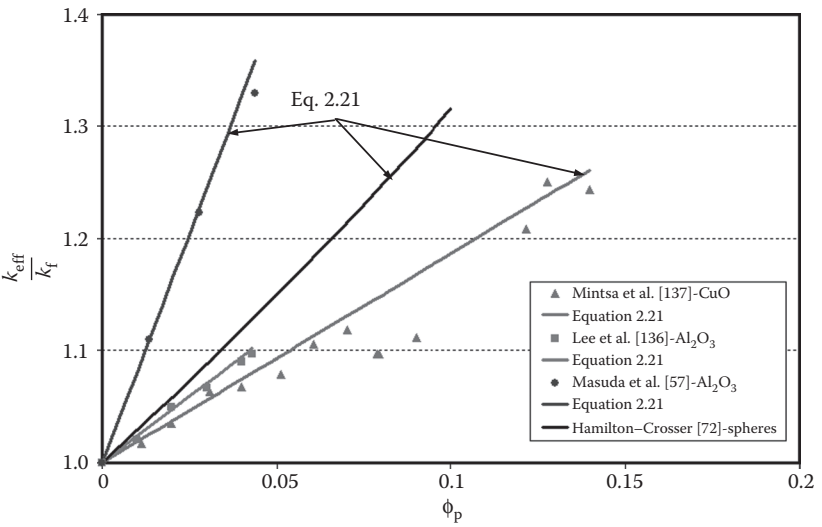

FIGURE 2.7 Comparison of the general correlation, Equation 2.21 developed by Khanafer and Vafai [39] with the experimental data (Al_2O_3–water, CuO–water) at room temperature . (Reprinted from K. Khanafer and K. Vafai. 2011, A critical synthesis of thermophysical characteristics of nanofluids, *International Journal of Heat and Mass Transfer* 54, 4410–4428, Copyright 2011, with permission from Elsevier.)

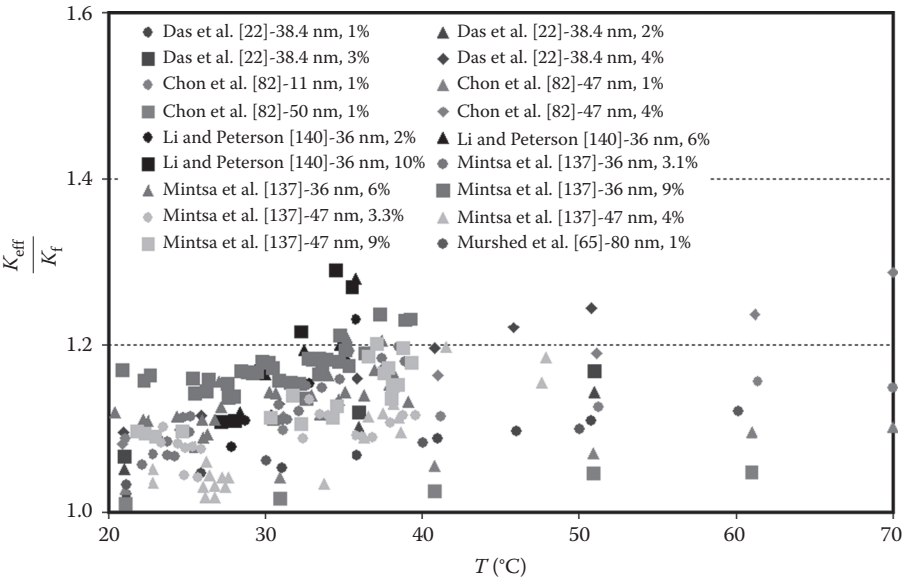

FIGURE 2.8 Comparison of the experimental data for the thermal conductivity enhancement of Al_2O_3–water nanofluid at different temperatures and volume fractions. (Reprinted from K. Khanafer and K. Vafai. 2011, A critical synthesis of thermophysical characteristics of nanofluids, *International Journal of Heat and Mass Transfer* 54, 4410–4428, Copyright 2011, with permission from Elsevier.)

the nanofluid to the thermal conductivity of the base fluid at the same temperature) results of Al_2O_3–water nanofluid obtained from various experimental results as a function of volume fraction and nanoparticle's diameter. Figure 2.8 illustrates that temperature has an important effect on the thermal conductivity augmentation.

A general correlation was developed by Khanafer and Vafai [39] for Al_2O_3–water nanofluid using the available experimental data at various temperatures, nanoparticle's diameter, and volume fraction. The developed correlation was given in terms of nanoparticle's diameter, volume fraction, dynamic viscosity of water, effective dynamic viscosity of the nanofluid, and temperature as follows:

$$\frac{k_{eff}}{k_f} = 0.9843 + 0.398\phi_p^{0.7383}\left(\frac{1}{d_p(\text{nm})}\right)^{0.2246}\left(\frac{\mu_{eff}(T)}{\mu_f(T)}\right)^{0.0235} - 3.9517\frac{\phi_p}{T} + 34.034\frac{\phi_p^2}{T^3} + 32.509\frac{\phi_p}{T^2} \tag{2.22}$$

$$0 \le \phi_p \le 10\%, 11\,\text{nm} \le d \le 150\,\text{nm}, 20\,^\circ\text{C} \le T \le 70\,^\circ\text{C}$$

where the dynamic viscosity (Pa.s) of water at different temperatures can be expressed as

$$\mu_f(T) = 2.414 \times 10^{-5} \times 10^{247.8/(T-140)} \tag{2.23}$$

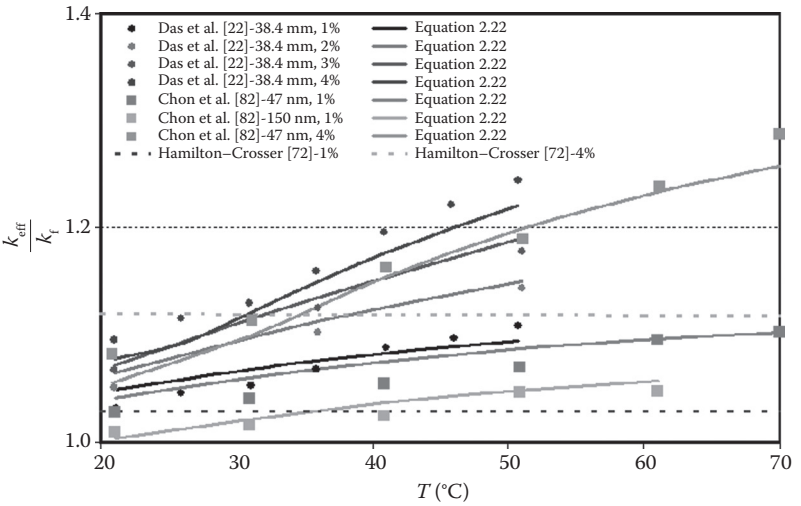

FIGURE 2.9 Comparison of the general correlation, Equation 2.22 developed by Khanafer and Vafai [39] with the experimental data (Al_2O_3–water) at various temperatures and volume fractions. (Reprinted from K. Khanafer and K. Vafai. 2011, A critical synthesis of thermophysical characteristics of nanofluids, *International Journal of Heat and Mass Transfer* 54, 4410–4428, Copyright 2011, with permission from Elsevier.)

where T in Kelvin. Figure 2.9 shows a very good agreement between the predicted relative effective thermal conductivity by Khanafer and Vafai [39] model and the experimental data.

Different models were developed in the literature for the effective thermal conductivity of a two-component mixture such as the Hamilton and Crosser model [72]. Although this model gave a good approximation for the effective thermal conductivity of the Al_2O_3–water and CuO–water nanofluids for small volume fractions at room temperature, it does not exhibit a good approximation of the effective thermal conductivity at various temperatures as depicted in Figure 2.9 because this model [72] as well as a number of other models in this area do not properly account for the variations of the effective thermal conductivity with temperature. Therefore, these analytical models cannot be used to estimate the effective thermal conductivity of nanofluids at various temperatures. Instead, Equation 2.22 developed by Khanafer and Vafai [39] may be used to give a better estimation of the effective thermal conductivity of Al_2O_3–water nanofluids at various temperatures.

2.5 NUCLEATE POOL BOILING AND CRITICAL HEAT FLUX OF NANOFLUIDS

Boiling heat transfer plays a significant role in a variety of technological and industrial applications such as heat exchangers, microchannel-cooling applications, cooling of high-power electronics and nuclear reactors. The use of nanofluids in enhancing boiling heat-transfer characteristics is of great interest [83,84,42]. Several experimental

studies on the nucleate pool boiling and critical heat flux (CHF) characteristics of nanofluids have been conducted in the literature [18,85–96]. Conflicting results on the effect of nanoparticles on the nucleate boiling heat-transfer rate and CHF were reported. For example, Das et al. [21,22] conducted an experimental study on pool boiling characteristics of Al_2O_3–water nanofluids on smoother and roughened heating surfaces for various particle concentrations. Their results show that nanoparticles degraded the boiling performance with increasing particle concentration. You et al. [86] found that nucleate boiling heat-transfer coefficient remained unchanged with the addition of Al_2O_3 nanoparticles compared with water. Bang and Chang [87] experimentally studied boiling heat transfer characteristics of nanofluids on a smooth horizontal flat surface with nanoparticles suspended in water using different volume concentrations of Al_2O_3 nanoparticles. Their experimental results showed that nanofluids have poor heat-transfer performance compared with pure water in natural convection and nucleate boiling. Contrary to the above results, an experimental investigation into the pool boiling heat transfer of aqueous based γ-alumina nanofluids (primary particle size 10–50 nm) was carried out by Wen and Ding [18]. The results showed that alumina nanofluids can significantly enhance boiling heat transfer. The enhancement was shown to increase with increasing particle concentration up to approximatley 40% at a particle loading of 1.25% by weight. Ding et al. [27] showed that the boiling heat transfer was enhanced in the nucleate regime for both alumina and titania (TiO_2) nanofluids, and the enhancement is more sensitive to the concentration change for TiO_2 nanofluids.

Most CHF experimental studies using nanofluids have shown CHF enhancement under pool boiling conditions [86,87,91,92]. You et al. [86] investigated experimentally the effect of Al_2O_3 nanoparticles (tested concentrations of nanoparticles range from 0 to 0.05 g/L) on CHF of water in pool boiling. The measured pool boiling curves of nanofluids saturated at 60°C have demonstrated that the CHF increases dramatically (approximately 200%) compared with that of pure water. Kim et al. [91] conducted an experimental study on the CHF characteristics of nanofluids in pool boiling. Their results illustrated that the CHF of nanofluids containing TiO_2 or Al_2O_3 were enhanced up to 100% over that of pure water. Vassallo et al. [93] experimentally demonstrated a marked increase in the CHF (up to 60%) for both nano- and microsolutions (silica–water) at the same concentration (0.5% volume fraction) compared with the base water. Bang and Chang [87] show that CHF performance using Al_2O_3–water nanofluids was enhanced to 32% and 13%, respectively, for both horizontal and vertical flat surfaces in the pool. They related the enhancement in CHF to the change of surface characteristics by the deposition of nanoparticles. Milanova and Kumar [97] conducted an experimental study to measure heat transfer characteristics of silica nanofluids at different acidity and base for various ionic concentrations in a pool boiling condition. They showed that nano-silioca suspensions increased the CHF by 200% times compared to when only pure water is utilized. In addition, they reported that nanofluids in a strong electrolyte exhibit a higher CHF than in buffer solutions because of the difference in surface areas. Figure 2.10 demonstrates a comparison of CHF enhancements between experimental results for various volume concentrations and nanoparticle material and diameter. Table 2.8 gives a summary of research studies on nucleate pool boiling heat transfer coefficient and CHF of nanofluids.

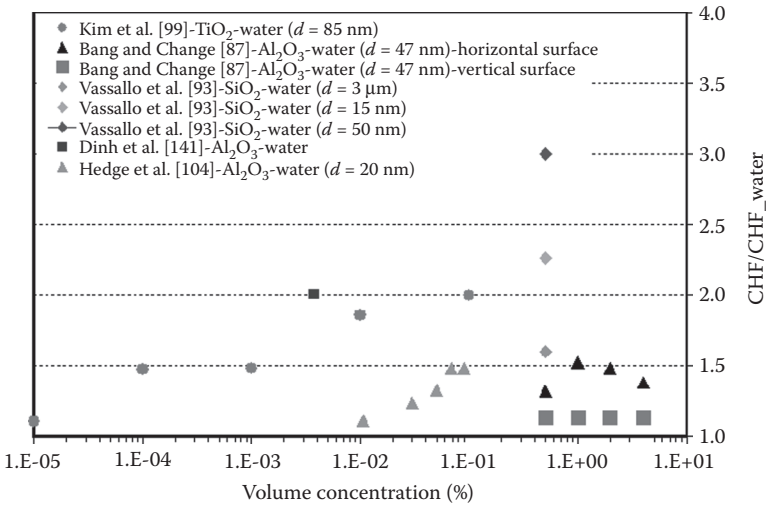

FIGURE 2.10 Comparison of CHF enhancements between experimental results for various volume concentrations, nanoparticles materials, and nanoparticles diameter.

2.5.1 Nucleate Pool Boiling Heat Transfer and CHF Enhancement Mechanisms of Nanofluids

A number of investigations have been carried out to explore the augmentation mechanisms or deterioration of nucleate pool boiling heat-transfer coefficient using nanofluids. These mechanisms include development of nanoparticles coatings on the surface during pool boiling of nanofluids [87], decrease in active nucleation sites due to nanoparticle sedimentation on the boiling surface [103], and the wettability change of the surface [21,22]. The presented experimental results on nucleate pool boiling heat-transfer coefficient of nanofluids are in disagreement. Although the CHF enhancement results by nanofluids are consistent in the literature, the responsible mechanisms are not well established. For example, Golubovic et al. [101] concluded that the main reason behind the increase of CHF in pool boiling of nanofluids is a decrease in the static surface contact angle.

Many other studies consider the major reason for CHF augmentation is due to the surface coating effect [87,88,93,95,96,104,105]. For example, Bang and Chang [87] carried out an experimental study on boiling heat transfer characteristics of nanofluids with nanoparticles suspended in water using different concentrations of alumina nanoparticles (Al_2O_3). The CHF performance was improved for both horizontal (32%) and vertical (13%) flat surfaces and the authors associated this augmentation to a change of surface characteristics by the deposition of nanoparticles. If this reasoning is accepted, it might be easier to alter the boiling surface in pursuit of a greater number of nucleation sites per area rather than using nanofluids [106,107]. Anderson and Mudawar [106] demonstrated that the surfaces with microgrooves and square microstuds are highly effective in improving the nucleate boiling heat-transfer coefficient in Fluorinert electronic liquid (FC-72) resulting and increase in CHF values

TABLE 2.8
Summary of Research Studies on Nucleate Pool Boiling Heat Transfer Coefficient (BHT) and CHF of Nanofluids

Reference	Nanofluids	Remarks
Das et al. [21,22]	Al_2O_3–water	BHT degradation
Chopkar et al. [98]	ZrO_2–water	BHT enhancement at low-volume fraction of nanoparticles (<0.07%) BHT degradation (>0.07%)
You et al. [86]	Al_2O_3–water	No change in BHT coefficient CHF enhancement up to 200%
Bang and Chang [87]	Al_2O_3–water	BHT degradation CHF enhancement up to 32%
Wen and Ding [89]	γ-Al_2O_3–water	BHT enhancement up to 40%
Liu et al. [90]	Carbon nanotube, deionized water	Both BHT and CHF enhancement Decrease in pressure, increase in BHT and CHF enhancement
Ding et al. [27]	Al_2O_3–water TiO_2–water	BHT enhancement for both TiO_2 and Al_2O_3
Kim et al. [91]	TiO_2–water Al_2O_3–water	CHF enhancement up to 100%
Kim et al. [99]	TiO_2–water	CHF enhancement up to 200%
Vassallo et al. [93]	SiO_2–water	No change in BHT coefficient CHF enhancement up to 60%
Milanova and Kumar [97]	SiO_2–water (also in salt and strong electrolyte solution)	CHF enhancement: three times greater than pure water
Milanova and Kumar [100]	SiO_2–water	CHF enhancement: 50% with no nanoparticle deposition on wire
Golubovic et al. [101]	Al_2O_3–water, Bismuth oxide (Bi_2O_3)–water	CHF enhancement: up to 50% for Al_2O_3 and 33% for Bi_2O_3
Kwark et al. [102]	Al_2O_3–water, CuO–water, and diamond–water	BHT degradation CHF enhancement: increases with nanoparticles concentration until reaches an asymptotic value

by up to 2.5 times compared with a smooth surface. Honda et al. [108] and Wei et al. [109] illustrated that CHF values for the nano-roughened surface and micro-pin-finned surfaces were, respectively, 1.8 to 2.2 and 2.3 times those for a smooth silicon surface. Ujereh et al. [110] conducted experiments to evaluate the impact of coating silicon and copper substrates with nanotubes on pool boiling characteristics. Fully coating the substrate surface with carbon nanotubes was found to be highly effective at reducing the incipience superheat and significantly enhancing both the nucleate boiling heat-transfer coefficient and CHF.

More robust physical models are necessary to elucidate the influence of nanofluids on nucleate pool boiling and CHF. Detailed understanding of the thermophysical properties of nanofluids, coating of nanoparticles, and structure of the boiling

surface can be helpful in resolving the controversies in the pool boiling heat-transfer coefficient of nanofluids as well as in illustrating the mechanisms that results in a substantial increase in CHF.

2.5.2 Nucleate Pool Boiling Heat Transfer and CHF Correlations

A number of studies in the literature have presented correlations in the absence of nanoparticles to explain the causes of CHF increase. Zuber's correlation [111], which was largely utilized to predict CHF for an infinite flat plate in the absence of nanoparticles is given by

$$q''_{\mathrm{CHF,Zuber}} = 0.131 h_{\mathrm{fg}} \rho_g^{1/2} \left[g\sigma\left(\rho_{\mathrm{f}} - \rho_g\right)\right]^{1/4} \tag{2.24}$$

where σ is the surface tension, ρ_{f} and ρ_g are the liquid and vapor densities respectively, and h_{fg} is the latent heat. According to the above correlation, densities of liquid and vapor, surface tension, and heat of vaporization may affect CHF values. Later Lienhard and Dhir [112] modified Zuber's correlation to account for both size and geometrical effects. They provided hydrodynamic predictions of CHF from different finite bodies

$$q''_{\mathrm{CHF}} = 0.149 h_{\mathrm{fg}} \rho_g^{1/2} \left[g\sigma\left(\rho_{\mathrm{f}} - \rho_g\right)\right]^{1/4} \tag{2.25}$$

This correlation shows that CHF is proportional to surface tension $\sigma^{1/4}$. This effect is rather weak. Kandlikar [113] extended Zuber's correlation to include the effect of contact angle (β) as follows:

$$\frac{q''_{\mathrm{CHF}}}{h_{\mathrm{fg}} \rho_g^{1/2} \left[g\sigma\left(\rho_{\mathrm{f}} - \rho_g\right)\right]^{1/4}} = \left(\frac{1+\cos\beta}{16}\right)\left[\frac{\pi}{4}\left(1+\cos\beta\right) + \frac{2}{\pi}\right]^{1/2} \tag{2.26}$$

There are many studies reported in the literature associated with the effects of heating surface conditions on the pool boiling CHF. Ramilison et al. [114] studied the influence of surface conditions such as roughness and contact angle on CHF. Ramilison et al. [114] suggested the following correlation:

$$\frac{q''_{\mathrm{CHF}}}{q''_{\mathrm{CHF,Zuber}}} = A\left(\pi - \beta_{\mathrm{r}}\right)^B \left(r\right)^{\left(C + D\beta_{\mathrm{r}}\right)} \tag{2.27}$$

where β_{r} is the receding contact angle and r is the rms value of surface roughness. The above correlation shows that CHF is directly proportional to the surface roughness. Following a dimensional analysis, Kutateladze [115,116] proposed a correlation based on assumption that the critical condition is reached when

the velocity in the vapor phase reaches a critical value. This correlation can be expressed as

$$\frac{q''_{\mathrm{CHF}}}{h_{\mathrm{fg}}\rho_g^{1/2}\left[g\sigma\left(\rho_{\mathrm{f}}-\rho_g\right)\right]^{1/4}} = K \tag{2.28}$$

The value of K was found to be 0.16 from the experimental data.

Borishanskii [117] obtained an analytical expression for the constant K in Kutateladze correlation as

$$K = 0.13 + 4\left\{\frac{\rho_{\mathrm{f}}\sigma^{3/2}}{\mu^2\left[g\left(\rho_{\mathrm{f}}-\rho_g\right)\right]^{1/2}}\right\}^{-0.4} \tag{2.29}$$

Bubble crowding at heated surface was proposed by Rosenhow and Griffith [118]. They assumed that increased packing of the heating surface with bubbles at higher heat fluxes is responsible for stopping the flow of liquid to the heating surface leading to CHF. They proposed the following equation for CHF

$$\frac{q''_{\mathrm{CHF}}}{h_{\mathrm{fg}}\rho_g} = C_1\left(\frac{g}{g_{\mathrm{s}}}\right)^{1/4}\left[\frac{\rho_{\mathrm{f}}-\rho_g}{\rho_g}\right]^{0.6} \tag{2.30}$$

where $C_1 = 0.012$ m/s, g is the local gravitational acceleration, and g_{s} corresponds to the standard g value. Chang [119] considered the forces acting on the bubble and assumed that the CHF condition was achieved when the Weber number reached a critical value. The following correlation was developed by Chang [119] for vertical surfaces

$$q''_{\mathrm{CHF}} = 0.098h_{\mathrm{fg}}\rho_g^{1/2}\left[g\sigma\left(\rho_{\mathrm{f}}-\rho_g\right)\right]^{1/4} \tag{2.31}$$

One can note from above correlations that the CHF depends on the physical properties such as surface tension, liquid and vapor densities, and viscosity as well as bubble dynamics and nucleation density site. Furthermore, structure of boiling surface and thermophysical properties of nanofluids may also affect nucleate boiling heat transfer and CHF.

2.6 MEDICAL APPLICATIONS OF NANOPARTICLES

The applications of nanoscience and nanotechnology in medicine, especially in diagnosis and treatment of diseases, have received considerable attention by many researchers and pharmaceutical companies [120]. One of the applications includes

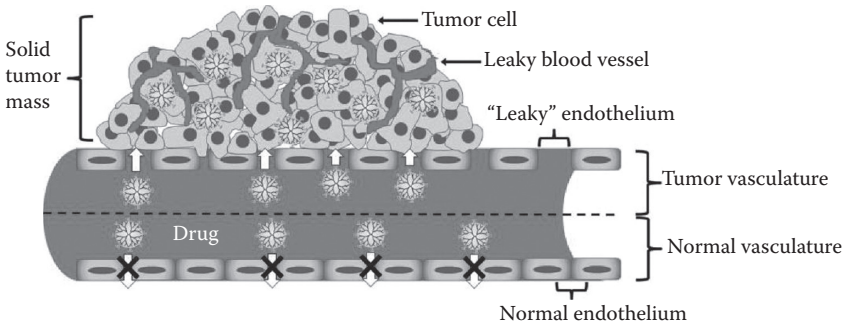

FIGURE 2.11 Diffusion of dendrimes-based drug-delivery systems across the tumor's leaky vasculature into the tumor tissue. (Reprinted with permission from S.H. Madina and M.E. El-Sayed. 2009, Dendrimers as carriers for delivery of chemotherapeutic agents, *Chem Rev.* 109, 3141–3157, Copyright 2009, with permission from ACS Publications.)

the use of nanoparticles (1–100 nm) in drug and gene delivery [121,122], detection of proteins [123], probing of DNA structure [124], tissue engineering [125], magnetic resonance imaging contrast enhancement [126], and tumor destruction via hyperthermia [127]. Nanoparticles have distinctive physicochemical properties such as ultra small size, large surface to mass ratio, high reactivity, and unique interactions with biological systems [128]. In drug-delivery applications, controlled-released drugs delivered to the site of action at a designed rate have numerous advantages over the conventional dosage forms. This interest stems from its importance in reducing dosing frequency, adverse side effects, and in achieving improved pharmacological activity as well as in maintaining constant and prolonged therapeutic effects [129,130]. Nanoparticles are engineered to bind to target cells and deliver high doses of therapeutic compounds which results in reducing damage to healthy cells in the body [122] (Figure 2.11). Nanoparticles used as drug delivery systems are made using a variety of materials such as polymers (polymeric nanoparticles, micelles, or dendrimers), lipids, viruses, and organometallic compound (nanotubes) [131]. Figure 2.12 shows a schematic diagram showing the composition of liposomes, dendrimers,

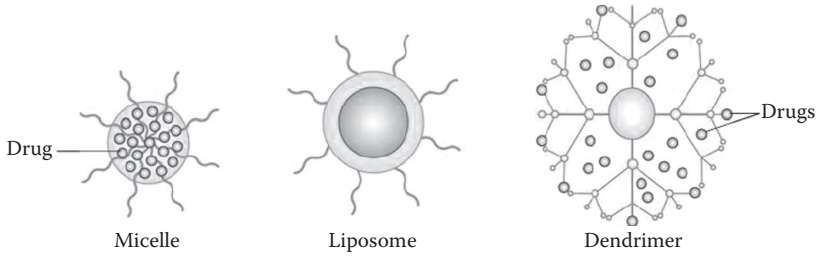

FIGURE 2.12 Schematic diagram of nanoparticles used as drug delivery systems. (Reprinted with kind permission from Springer: ElHazzat Jallal and E.H. El-Sayed Mohamed. 2010, Advances in targeted breast cancer, *Current Breast Cancer Reports* 2, 146–151.)

and polymeric micelles used for delivery of chemotherapeutic agents for treatment of breast cancer [132].

Another application of nanoparticles can be found in imaging. Recent advances in nanoparticle technology have led to the implementation of nanoparticles such as TiO_2, quantum dots, and gold nanoparticles in cellular imaging due to their distinctive properties compared with traditional fluorescent dyes and proteins. For instance, the smaller size and improved photostability of quantum dots allow for prolonged and enhanced visualization of biological components in fixed cells [133].

2.7 CONCLUSIONS

Thermophysical properties of nanofluids and their importance in biomedical applications and heat-transfer enhancement are discussed in this study. General correlations for the effective thermal conductivity and viscosity of nanofluids are developed in this study based on the experimental data in terms of various pertinent parameters. The experimental data reported by many authors for the effective thermal conductivity and dynamic viscosity of nanofluids are in disagreement. This study has illustrated that the results of the effective thermal conductivity and viscosity of nanofluids can be determined at room temperature using the classical equations at low-volume fractions. However, these models cannot predict the thermal conductivity at other temperatures. Moreover, for high heat-flux applications, the experimental results reported in the literature showed contradictory results in pool boiling heat-transfer characteristics while the CHF of nanofluids demonstrates a significant increase with the addition of nanoparticles. This review summarizes some of the potential applications of nanoparticles in biomedical applications related to cancer treatment, medical imaging, and drug-delivery systems.

NOMENCLATURE

c_{eff}	heat capacity of nanofluids
c_f	heat capacity of the base fluid
c_p	heat capacity of nanoparticles
C	proportional constant
d_f	diameter of the fluid molecule
d_p	nanoparticles diameter
h	inter-particle spacing
h_{fg}	latent heat
k	thermal conductivity
k_B	Stefan–Boltzmann constant
k_{eff}	thermal conductivity of nanofluids
k_H	Huggins Coefficient
k_{layer}	thermal conductivity of the nano-layer
m	mass
n	empirical shape factor
Pr	Prandtl number
Re	Reynolds number

r	rms value of surface roughness
t	thickness of the nano-layer
T	temperature
V	volume

Greek Symbols

β	ratio of nano-layer thickness to radius of nanoparticle
β_{eff}	thermal expansion coefficient of nanofluids
β_f	thermal expansion coefficient of the base fluid
β_p	thermal expansion coefficient of nanoparticle
β_r	receding contact angle
ρ	density
ρ_{eff}	density of nanofluids
γ	ratio of nano-layer thermal conductivity to nanoparticle thermal conductivity
κ	ratio of nanoparticle thermal conductivity to fluid thermal conductivity
ψ	particle sphericity
ϕ_p	volume fraction of nanoparticles
$\phi_{p,max}$	maximum volume fraction of nanoparticles
μ_{eff}	dynamic viscosity of nanofluids
μ_f	dynamic viscosity of the base fluid
$\mu_{Brownian}$	dynamic viscosity due to Brownian motion
σ	surface tension

Subscripts

f	fluid
p	nanoparticle

REFERENCES

1. S.U.S. Choi. Nanofluids: From vision to reality through research, *Journal of Heat Transfer* 131, 2009, 1–9.
2. K.V. Wong and O. Leon. Applications of nanofluids: Current and future, *Advances in Mechanical Engineering.* 2010, 1–11.
3. V. Bianco, F. Chiacchio, O. Manca, and S. Nardini. Numerical investigation of nanofluids forced convection in circular tubes, *Applied Thermal Engineering* 29, 2009, 3632–3642.
4. M. Shafahi, V. Bianco, K. Vafai, and O. Manca. Thermal performance of flat-shaped heat pipes using nanofluids, *International Journal of Heat and Mass Transfer* 53, 2010, 1438–1445.
5. M. Shafahi, V. Bianco, K. Vafai, and O. Manca. An investigation of the thermal performance of cylindrical heat pipes using nanofluids, *International Journal of Heat and Mass Transfer* 53, 2010, 376–383.
6. K. Khanafer, K., Vafai, and M. Lightstone. Buoyancy-driven heat transfer enhancement in a two-dimensional enclosure utilizing nanofluids, *International Journal of Heat and Mass Transfer* 46, 2003, 3639–3653.
7. A.R.A. Khaled and K. Vafai, Heat transfer enhancement through control of thermal dispersion effects, *International Journal of Heat and Mass Transfer* 48, 2005, 2172.

8. J.A. Eastman, S.U.S. Choi, S. Li, L.J. Thompson, and S. Lee. Enhanced thermal conductivity through the development of nanofluids. In: 1996 Fall meeting of the Materials Research Society (MRS), Boston, USA.
9. J.A. Eastman, S.U.S. Choi, S. Li, W. Yu, and L.J. Thompson. Anomalously increased effective thermal conductivities of ethylene glycol-based nanofluids containing copper nanoparticles, *Applied Physics Letters* 78, 2001, 718–720.
10. S.P. Jang and S.U.S. Choi. Role of Brownian motion in the enhanced thermal conductivity of nanofluids, *Applied Physics Letters* 84, 2004, 4316–4318.
11. S. Lee and S.U.S. Choi. Application of metallic nanoparticle suspensions in advanced cooling systems. In: 1996 International Mechanical Engineering Congress and Exhibition, Atlanta, USA.
12. A. Ali, K. Vafai, and A.-R.A. Khaled. Comparative study between parallel and counter flow configurations between air and falling film desiccant in the presence of nanoparticle suspensions, *International Journal of Energy Research* 27, 2003, 725–745.
13. N. Putra, W. Roetzel, and S.K. Das. Natural convection of nanofluids. *Heat and Mass Transfer* 39, 2003, 775–784.
14. Y.M. Xuan and Q. Li. Heat transfer enhancement of nanofluids, *International Journal of Heat and Fluid Flow* 21, 2000, 58–64.
15. Y.M. Xuan and Q. Li. Investigation on convective heat transfer and flow features of nanofluids, *ASME Journal of Heat Transfer* 125, 2003, 151–155.
16. B.C. Pak and Y.I. Cho. Hydrodynamic and heat transfer study of dispersed fluids with submicron metallic oxide particles, *Experimental Heat Transfer* 11, 1999, 151–170.
17. Y. Yang, Z. Zhang, E. Grulke, W. Anderson, and G. Wu, G. Heat transfer properties of nanoparticle-in-fluid dispersions (nanofluids) in laminar flow, *International Journal of Heat and Mass Transfer* 48, 2005, 1107–1116.
18. D.S. Wen and Y.L. Ding. Experimental investigation into the pool boiling heat transfer of aqueous based alumina nanofluids, *Journal of Nanoparticle Research* 7, 2005, 265–274.
19. B.X. Wang, L.P. Zhou, and X.F. Peng. A fractal model for predicting the effective thermal conductivity of liquid with suspension of nanoparticles, *International Journal of Heat and Mass Transfer* 46, 2003, 2665–2672.
20. S.K. Das, N. Putra, and W. Roetzel. Pool boiling characteristics of nanofluids, *International Journal of Heat and Mass Transfer* 46, 2003a, 851–862.
21. S.K. Das, N. Putra, and W. Roetzel. Pool boiling of nanofluids on horizontal narrow tubes, *International Journal of Multiphase Flow* 29, 2003b, 1237–1247.
22. S.K. Das, N. Putra, P. Thiesen, and W. Roetzel, Temperature dependence of thermal conductivity enhancement for nanofluids, *Journal Heat Transfer* 125, 2003, 567–574.
23. J. Kim, Y.T. Kang, and C.K. Choi. Analysis of convective instability and heat transfer characteristics of nanofluids, *Physics of Fluids* 16, 2004, 2395–2401.
24. B. Ghasemi and S.M. Aminossadati. Natural convection heat transfer in an inclined enclosure filled with a water-CuO nanofluid, *Numerical Heat Transfer, Part A* 55, 2009, 807–823.
25. A.G.A. Nnanna, T. Fistrovich, K. Malinski, and S.U.S. Choi. Thermal transport phenomena in buoyancy-driven nanofluids, in *Proceedings of 2005 ASME International Mechanical Engineering Congress and RD&D Exposition*, November 15–17, 2004, Anaheim, CA, USA.
26. A.G.A. Nnanna and M. Routhu. Transport phenomena in buoyancy-driven nanofluids—Part II, *in Proceedings of 2005 ASME Summer Heat Transfer Conference*, July 17–22, 2005, San Francisco, California, USA.
27. Y. Ding, H. Chen, L. Wang et al., Heat transfer intensification using nanofluids, *Journal of Particle and Powder* 25, 2007, 23–36.

28. B.H. Chang, A.F. Mills, and E. Hernandez. Natural convection of micro-particle suspensions in thin enclosures, *International Journal of Heat and Mass Transfer* 51, 2008, 1332–1341.
29. P. Keblinski, S.R. Phillpot, S.U.S. Choi, and J.A. Eastman. Mechanisms of heat flow in suspensions of nano-sized particles (nanofluids), *International Journal of Heat and Mass Transfer* 45, 2002, 855–863.
30. J.A. Eastman, S.R. Phillpot, S.U.S. Choi, and P. Keblinski. Thermal transport in nanofluids, *Annual Review Of Materials Research* 34, 2004, 219–246.
31. W. Evans, J. Fish, and P. Keblinski. Role of Brownian motion hydrodynamics on nanofluid thermal conductivity, *Applied Physics Letters* 88(9), 2006, 93116.
32. W. Yu and S.U.S. Choi. The role of interfacial layers in the enhanced thermal of nanofluids: a renovated Maxwell model, *Journal of Nanoparticle Research* 5 (1–2), 2003, 167–171.
33. W. Yu and S.U.S. Choi, The role of interfacial layers in the enhanced thermal conductivity of nanofluids: A renovated Hamilton–Crosser model, *Journal of Nanoparticle Research* 6(4), 2004, 355–361.
34. Q. Xue and W.M. Xu. A model of thermal conductivity of nanofluids with interfacial shells, *Materials Chemistry and Physics* 90, 2005, 298–301.
35. Q. Xue. Model for effective thermal conductivity of nanofluids, *Physics Letters A* 307, 2003, 313–317.
36. H. Xie, M. Fujii, and X. Zhang. Effect of interfacial nanolayer on the effective thermal conductivity of nanoparticle-fluid mixture, *International Journal of Heat and Mass Transfer* 48, 2005, 2926–2932.
37. L. Xue, P. Keblinski, S.R. Phillpot, S.U.S. Choi, and J.A. Eastman. Effect of liquid layering at the liquid–solid interface on thermal transport, *Int. J. Heat Mass Transfer* 47(19–20), 2004, 4277–4284.
38. C.J. Ho, W.K. Liu, Y.S. Chang, and C.C. Lin. Natural convection heat transfer of alumina-water nanofluid in vertical square enclosures: An experimental study, *International Journal of Thermal Sciences* 49, 2010, 1345–1353.
39. K. Khanafer and K. Vafai. A critical synthesis of thermophysical characteristics of nanofluids, *International Journal of Heat and Mass Transfer* 54, 2011, 4410–4428.
40. S.P. Jang and S.U. Choi. Free convection in a rectangular cavity (Benard Convection) with nanofluids, *Proceedings of the 2004 ASME International Mechanical Engineering Congress and Exposition*, Anaheim, California, November 13–20.
41. L. Gosselin and A.K. da Silva. Combined heat transfer and power dissipation optimization of nanofluid flows, *Applied Physics Letters* 85, 2004, 4160.
42. J. Lee and I. Mudawar. Assessment of the effectiveness of nanofluids for single-phase and two-phase heat transfer in micro-channels, *International Journal of Heat and Mass Transfer* 50, 2007, 452–463.
43. S.Q. Zhou and R. Ni. Measurement of the specific heat capacity of water-based Al_2O_3 nanofluid, *Applied Physics Letters* 92, 2008, 093123.
44. K.S. Hwang, J.H. Lee, and S.P. Jang, Buoyancy-driven heat transfer of water-based Al2O3 nanofluids in a rectangular cavity, *International Journal of Heat and Mass Transfer* 50, 2007, 4003–4010.
45. C.J. Ho, M.W. Chen, and Z.W. Li. Numerical simulation of natural convection of nanofluid in a square enclosure: Effects due to uncertainties of viscosity and thermal conductivity, *International Journal of Heat and Mass Transfer* 51, 2008, 4506–4516.
46. A. Einstein. Eine neue bestimmung der molekuldimensionen, *Annalen der Physik, Leipzig*, 19, 1906, 289–306.
47. H.C. Brinkman. The viscosity of concentrated suspensions and solutions. *J. Chem Phys* 20, 1952, 571.

48. G. Batchelor. The effect of Brownian motion on the bulk stress in a suspension of spherical particles, *J. Fluid Mechanics* 83, 1977, 97–117.
49. T. Lundgren. Slow flow through stationary random beds and suspensions of spheres, *J. Fluid Mechanics* 51, 1972, 273–299.
50. A.L. Graham. On the viscosity of suspensions of solid spheres, *Appl. Sci. Res*. 37, 1981, 275–286.
51. R.A. Simha. Treatment of the viscosity of concentrated suspensions, *Journal of Applied Physics* 23, 1952, 1020–1024.
52. M. Mooney. The viscosity of a concentrated suspension of spherical particles, *Journal of Colloid Science* 6, 1951, 162–170.
53. V.H. Eilers. Die viskocitat von emulsionen hochviskoser stoffe als funktion der konzentration, *Kolloid-Zeitschrift* 97, 1941, 313–321.
54. N. Saito. Concentration dependence of the viscosity of high polymer solutions, *Journal of Physical Society of Japan* 5, 1950, 4–8.
55. N.A. Frankel and A. Acrivos. On the viscosity of a concentrate suspension of solid spheres, *Chemical Engineering Science* 22, 1967, 847–853.
56. X. Wang, X. Xu, and S.U.S. Choi. Thermal conductivity of nanoparticles–fluid mixture, *Journal of Thermophysics Heat Transfer* 13, 1999, 474–480.
57. H. Masuda, A. Ebata, K. Teramae, and N. Hishinuma. Alteration of thermal conductivity and viscosity of liquid by dispersing ultra-fine particles (dispersion of c-Al_2O_3, SiO_2 and TiO_2 ultra-fine particles), *Netsu Bussei* 4, 1993, 227–233.
58. S. Maiga, S.J. Palm, C.T. Nguyen, G. Roy, and N. Galanis. Heat transfer enhancement by using nanofluids in forced convection flows, *International Journal of Heat and Fluid Flow* 26, 2005, 530–546.
59. S. Maiga, C.T. Nguyen, N. Galanis, G. Roy, T. Mar'e, and M. Coqueux. Heat transfer enhancement in turbulent tube flow using Al2O3 nanoparticle suspension. In: Lewis, R.W. (Eds.), *International Journal of Numerical Methods Heat and Fluid Flow* 16, 2006, 275–292.
60. P.K. Namburua, D.P. Kulkarni, D. Misra, and D.K. Das. Viscosity of copper oxide nanoparticles dispersed in ethylene glycol and water mixture, *Experimental Thermal Fluid Science* 32, 2007, 397–402.
61. C.T. Nguyen, F. Desgranges, G. Roy, N. Galanis, T. Mare, S. Boucher, and H.A. Mintsa. Temperature and particle-size dependent viscosity data for water-based nanofluids–hysteresis phenomenon, *International Journal of Heat and Fluid Flow* 28, 2007, 1492–1506.
62. W.J. Tseng and K.C. Lin, Rheology and colloidal structure of aqueous TiO2 nanoparticle suspensions, *Materials Science and Engineering* A355, 2003, 186–192.
63. D.P. Kulkarni, D.K. Das, and S.L. Patil. Effect of temperature on rheological properties of copper oxide nanoparticles dispersed in propylene glycol and water mixture, *Journal of Nanosciense and Nanotechnology* 7, 2007, 2318–2322.
64. D.P. Kulkarni, D.K. Das, and G. Chukwa. Temperature dependent rheological of copper oxide nanoparticles suspension (nanofluid), *Journal of Nanosciense and Nanotechnology* 6, 2006, 1150–1154.
65. S.M.S. Murshed, K.C. Leong, and C. Yang. Investigations of thermal conductivity and viscosity of nanofluids, *International Journal of Thermal Sciences* 47, 2008, 560–568.
66. J. Buongiorno. Convective transport in nanofluids ASME, *Journal of Heat Transfer* 128, 2006, 240–250.
67. S.J. Palm, G. Roy, and C.T. Nguyen, Heat transfer enhancement with the use of nanofluids in radial flow cooling systems considering temperature-dependent properties, *Applied Thermal Engineering* 26, 2006, 2209–2218.

68. W. Duangthongsuk and S. Wongwises. Measurement of temperature-dependent thermal conductivity and viscosity of TiO_2-water nanofluids, *Experimental Thermal and Fluid Science* 33, 2009, 706–714.
69. P. K. Namburu, D.K. Das, K.M. Tanguturi, and R.S. Vajjha. Numerical study of turbulent flow and heat transfer characteristics of nanofluids considering variable properties, *International Journal of Thermal Sciences* 48, 2009, 290–302.
70. J. Koo and C. Kleinstreuer, Laminar nanofluid flow in microheat-sinks, *International Journal of Heat and Mass Transfer* 48, 2005, 2652–2661.
71. K.B. Anoop, S. Kabelac, T. Sundararajan, and S.K. Das. Rheological and flow characteristics of nanofluids: Influence of electroviscous effects and particle agglomeration, *Journal of Applied Physics* 106, 2009, 034909.
72. R.L. Hamilton and O.K. Crosser. Thermal conductivity of heterogeneous two-component systems, *I&EC Fundam* 1, 1962, 182–191.
73. J.C.A. Maxwell *Treatise on Electricity and Magnetism*. Clarendon Press, Oxford, UK, 2nd edition, 1881.
74. D.A.G. Bruggeman. Berechnung verschiedener physikalischer konstanten von heterogenen substanzen, I. Dielektrizitatskonstanten und leitfahigkeiten der mischkorper aus isotropen substanzen, *Annalen der Physik, Leipzig*, 24, 1935, 636–679.
75. F.J. Wasp. *Solid-Liquid Slurry Pipeline Transportation*, 1977, Trans. Tech., Berlin, Germany.
76. D.J. Jeffrey. Conduction through a random suspension of spheres, *Proceedings of Royal Society (London)* A335, 1973, 355–367.
77. R.H. Davis. The effective thermal conductivity of a composite material with spherical inclusions, *International Journal of Thermophysics* 7, 1986, 609–620.
78. S. Lu and H. Lin. Effective conductivity of composites containing aligned spherical inclusions of finite conductivity, *Journal of Applied Physics* 79, 1996, 6761–6769.
79. Y. Xuan, Q. Li, and W. Hu. Aggregation structure and thermal conductivity of nanofluids, *AIChE Journal* 49(4). 2003, 1038–1043.
80. R. Prasher, P. Bhattacharya, and P.E. Phelan. Thermal conductivity of nanoscale colloidal solutions (nanofluids), *Physical Review Letters* 94(2), 2005, 025901.
81. J. Koo, and C. Kleinstreuer. A new thermal conductivity model for nanofluids, *Journal of Nanoparticle Research* 6(6). 2004, 577–588.
82. C.H. Chon, K.D. Kihm, S.P. Lee, and S.U.S. Choi, Empirical correlation finding the role of temperature and particle size for nanofluid (Al_2O_3) thermal conductivity enhancement, *Applied Physics Letters* 87, 2005, 153107.
83. R.A. Taylor. Phelan PE: Pool boiling of nanofluids. Comprehensive review of existing data and limited new data, *International Journal of Heat and Mass Transfer* 52, 2009, 5339–5347.
84. H.S. Ahn, H. Kim, H. Jo, S. Kang, W. Chang, and M.H. Kim. Experimental study of critical heat flux enhancement during forced convective flow boiling of nanofluid on a short heated surface, *International Journal of Multiphase Flow* 36(5), 2010, 375–384.
85. G. Prakash Narayan, K.B. Anoop, and Sarit K. Das. Mechanism of enhancement/deterioration of boiling heat transfer using stable nanoparticle suspensions over vertical tubes, *Journal of Applied Physics* 102, 2007, 074317.
86. S.M. You, J.H. Kim, and K.H. Kim. Effect of nanoparticles on critical heat flux of water in pool boiling heat transfer, *Applied Physics Letters* 83, 2003, 3374–3376.
87. I.C. Bang and S.H. Chang. Boiling heat transfer performance and phenomena of Al2O3-water nanofluids from a plain surface in a pool, *International Journal Heat and Mass Transfer* 48, (2005) 2407–2419.
88. J.P. Tu, N. Dinh, and T. Theofanous. An experimental study of nanofluid boiling heat transfer, in *Proceedings of 6th International Symposium on Heat Transfer*, Beijing, China, 2004.
89. D.S. Wen, Y.L. Ding, and R.A. Williams. Pool boiling heat transfer of aqueous based TiO_2 nanofluids, *Journal of Enhanced Heat Transfer* 13, 2006, 231–244.

90. Z.H. Liu, J.G. Xiong, and R. Bao. Boiling heat transfer characteristics of nanofluids in a flat heat pipe evaporator with micro-grooved heating surface, *Int. J. Multiphase Flow* 33, 2007, 1284–1295.
91. M.H. Kim, J.B. Kim, and H.D. Kim, Experimental studies on CHF characteristics of nano-fluids at pool boiling, *International Journal of Multiphase Flow* 33, 2007, 691–706.
92. S.J. Kim, T. McKrell, J. Buongiorno, and L.W. Hu, Experimental study of flow critical heat flux in alumina–water, zinc-oxide–water and diamond-water nanofluids, *Journal of Heat Transfer* 131(4), 2009, 043204-1-7.
93. P. Vassallo, R. Kumar, and S.D. Amico. Pool boiling heat transfer experiments in silica–water nanofluids, *International Journal of Heat and Mass Transfer* 47, 2004, 407–411.
94. C.H. Li, B.X. Wang, and X.F. Peng. Experimental investigations on boiling of nanoparticle suspensions, in: *2003 Boiling Heat Transfer Conference*, 1993, Jamica, USA.
95. S.J. Kim, I.C. Bang, J. Buongiorno, and L.W. Hu. Effects of nanoparticle deposition on surface wettability influencing boiling heat transfer in nanofluids, *Applied Physics Letters* 89, 2006, 153107.
96. S.J. Kim, I.C. Bang, J. Buongiorno, and L. W. Hu. Surface wettability change during pool boiling of nanofluids and its effect on critical heat flux, *International Journal of Heat and Mass Transfer* 50, 2007, 4105–4116.
97. Milanova D, Kumar R. Role of ions in pool boiling heat transfer of pure and silica nanofluids, *Applied Physics Letters* 87(23), 2005, 233107-1-3.
98. M. Chopkar, A.K. Das, I. Manna, and P.K. Das. Pool boiling heat transfer characteristics of ZrO_2-water nanofluids from a flat surface in a pool, *Heat and Mass Transfer* 44(8), 2007, 999–1004.
99. H.D. Kim, J.H. Kim, and M.H. Kim. Experimental study on CHF characteristics of water-TiO_2 nanofluids, *Nuclear Engineering Technology* 38(1), 2006, 61.
100. D. Milanova and R. Kumar. Heat transfer behaviour of silica nanoparticles in pool boiling experiment, *J Heat Transf* 130(4), 2008, 1–6.
101. M. Golubovic, H.D.M. Hettiarachchi, W.M. Worek, and W.J. Minkowycz. Nanofluids and critical heat flux, experimental and analytical study, *Applied Thermal Engineering* 29, 2009, 1281–1288.
102. S.M. Kwark, R. Kumar, G. Moreno, J. Yoo, and S.M. You. Pool boiling characteristics of low concentration nanofluids, *International Journal of Heat and Mass Transf* 53, 2010, 972–981.
103. Z-H. Liu, X-F. Yang, and J-G. Xiong. Boiling characteristics of carbon nanotube suspensions under sub-atmospheric pressures, *International Journal of Thermal Science* 49(7), 2010, 1156–1164.
104. R. Hegde, S.S. Rao, and R.P. Reddy. Critical heat flux enhancement in pool boiling using Alumina nanofluids, *Heat Transfer, Heat Transfer—Asian Research* 39, 2010, 323–331.
105. K. Sefiane. On the role of structural disjoining pressure and contact line pinning in critical heat flux enhancement during boiling of nanofluids, *Applied Physics Letters* 89, 2006, 044106.
106. T.M. Anderson and I. Mudawar. Microelectronic cooling by enhanced pool boiling of a dielectric fluorocarbon liquid, *ASME Journal of Heat Transfer* 111, 1989, 752–759.
107. I. Mudawar and T.M. Anderson, Optimization of enhanced surfaces for high flux chip cooling by pool boiling, *ASME Journal of Electronic Package* 115, 1993, 89–99.
108. H. Honda, H. Takamastu, and J.J. Wei. Enhanced boiling of FC-72 on silicon chips with micro-pin-fins and submicron-scale roughness, *ASME Journal of Heat Transfer* 124, 2002, 383–389.
109. J.J. Wei, H. Honda, and L.J. Guo. Experimental study of boiling phenomena and heat transfer performances of FC-72 over micro-pin-finned silicon chips, *Heat and Mass Transfer* 41, 2005, 744–755.

110. S. Ujereh, T. Fisher, and I. Mudawar. Effects of carbon nanotube arrays on nucleate pool boiling, *International Journal of Heat and Mass Transfer* 50, 2007, 4023–4038.
111. N. Zuber. On the stability of boiling heat transfer, *ASME Journal of Heat Transfer* 80, 1958, 711–720.
112. J.H. Lienhard and V.K. Dhir. Hydrodynamic prediction of peak pool boiling heat fluxes from finite bodies, *ASME Journal of Heat Transfer* 95, 1973, 477–482.
113. S.J. Kandlikar. A theoretical model to predict pool boiling CHF incorporating effects of contact angle and orientation, *Journal of Heat Transfer* 123, 2001, 1071–1079.
114. J.M. Ramilison, P. Sadasivan, and J. H. Lienhard. Surface factors influencing burnout on flat heaters, *Jouranl of Heat Transfer* 114, 1992, 287.
115. S.S. Kutateladze. On the transition to film boiling under natural convection, *Kotloturbostroenie* 3, 1948, 10–12.
116. S.S. Kutateladze. A hydrodynamic theory of changes in a boiling process under free convection,' *Izvestia Akademia Nauk, S.S.S.R., Otdelenie Tekhnicheski Nauk* 4, 1951, 529.
117. V.M. Borishanskii. *On the Problem of Generalizing Experimental Data on the Cessation of Bubble Boiling in Large Volume of Liquids*, 1955, Ts. K.I.T., 28, Moscow.
118. W. Rosenhow and P. Griffith. Correlation ofmaximum heat flux data for boiling of saturated liquids, *Chemical Engineering Progress Symposium Series* 52, 1956, 47–49.
119. Y.P. Chang. An Analysis of the Critical Conditions and Burnout in Boiling Heat Transfer, USAEC Rep. TID-14004, 1961, Washington, DC.
120. W.H. De Jong and P. Borm. Drug delivery and nanoparticles: Applications and hazards, *International Journal of Nanomedicine* 3, 2008, 133–149.
121. D.J. Irvine. Drug delivery: One nanoparticle, on kill, *Nature Materials* 10, 2011, 342–343.
122. D. Panatarotto, C.D. Prtidos, J. Hoebeke, F. Brown, E. Kramer, J.P. Briand, S. Muller, M. Prato, and A. Bianco. Immunization with peptide-functionalized carbon nanotubes enhances virus-specific neutralizing antibody responses, *Chemistry & Biology* 10, 2003, 961–966.
123. J.M. Nam, C.C. Thaxton, and C.A. Mirkin. Nanoparticles-based bio-bar codes for the ultrasensitive detection of proteins, *Science* 301, 2003, 1884–1886.
124. R. Mahtab, J.P. Rogers, and C.J. Murphy. Protein-sized quantum dot luminescence can distinguish between "straight", "bent", and "kinked" oligonucleotides, *Journal of American Chemical Society* 117, 1995, 9099–9100.
125. J. Ma, H. Wong, L.B. Kong, and K.W. Peng. Biomimetic processing of nanocrystallite bioactive apatite coating on titanium, *Nanotechnology* 14, 2003, 619–623.
126. R. Weissleder, G. Elizondo, J. Wittenburg, C.A. Rabito, H.H. Bengele, and L. Josephson. Ultrasmall superparamagnetic iron oxide: Characterization of a new class of contrast agents for MR imaging, *Radiology* 175, 1990, 489–493.
127. J. Yoshida and T. Kobayashi. Intracellular hyperthermia for cancer using magnetite cationic liposomes, *Journal of Magnetism and Magnetic Materials* 194, 1999, 176–184.
128. L. Zhang, F.X. Gu, J.M. Chan, A.Z. Wang, R.S. Langer, and O.C. Farokhzad. Nanoparticles in medicine: Therapeutic applications and developments, *Clinical Pharmacology and Therapeutics* 83, 2008, 761–9.
129. Y.W. Chien. *Novel Drug Delivery Systems*, 2nd edn. Marcel Dekker, New York, 1992.
130. K. Khanafer and K. Vafai. The role of porous media in biomedical engineering as related to magnetic resonance imaging and drug delivery, *Heat and Mass Transfer* 42, 2006, 939–953.
131. K. Cho, X. Wang, S. Nie, Z. Chen, and D.M. Shin. Therapeutic nanoparticles for drug delivery in cancer, *Clinical Cancer Research* 14, 2008, 1310–1316.
132. ElHazzat Jallal and E.H. El-Sayed Mohamed. Advances in targeted breast cancer, *Current Breast Cancer Reports* 2, 2010, 146–151.

133. K. Thurn, E. Brown, A. Wu, S. Vogt, B. Lai, J. Maser, T. Paunesku, and G. Woloschak. Nanoparticles for applications in cellular imaging, *Nanoscale Research Letters* 2, 2007, 430–441.
134. S.H. Madina and M.E. El-Sayed. Dendrimers as carriers for delivery of chemotherapeutic agents, *Chem Rev*. 109, 2009, 3141–3157.